Hybrid particle-field molecular dynamics: a primer

Milano, G.; Sevink, G.J.A.; Lu, Z.Y.; Zhao, Y.; De Nicola, A.; Munaò, G.; ... ; Boyd, R.

Milano, Giuseppe, Sevink, G.J. Agur, Lu, Zhong-Yuan, Zhao, Ying, De Nicola, Antonio, Munaò, Gianmarco and Kawakatsu, Toshihiro (2024) Hybrid Particle-Field Molecular Dynamics: A Primer. In: Yanez, Manuel and Boyd, Russell J. (eds.) *Comprehensive Computational Chemistry,* vol. 3, pp. 636–659. Oxford: Elsevier.

http://dx.doi.org/10.1016/B978-0-12-821978-2.00109-4

Hybrid Particle-Field Molecular Dynamics: A Primer

Giuseppe Milano, Department of Chemical, Materials and Production Engineering, University of Naples Federico II, Napoli, Italy
GJ Agur Sevink, Leiden Institute of Chemistry, Leiden University, Leiden, Netherlands
Zhong-Yuan Lu, State Key Laboratory of Supramolecular Structure and Materials, College of Chemistry, Jilin University, Changchun, China
Ying Zhao, Institute of Nano-photonics, School of Physics and Materials Engineering, Dalian Minzu University, Dalian, China
Antonio De Nicola, Scuola Superiore Meridionale, Napoli, Italy
Gianmarco Munaò, Department of Mathematical and Computer Sciences, Physical Sciences and Earth Sciences, University of Messina, Messina, Italy
Toshihiro Kawakatsu, Department of Physics, Tohoku University, Sendai, Japan

Abstract

This chapter provides an introduction to Hybrid Particle-Field Molecular Dynamics (hPF-MD), the basic theoretical framework and the main ideas behind this recent methodology. The original implementation of hPF-MD in the massively parallel OCCAM code and the parallelization strategy is also described together with several early applications to biologically oriented problems (biomembranes, surfactants, drug delivery, bacterial lipids) and to materials science (polymers, nanocomposites, interfaces). The chapter ends with a discussion about open issues and perspectives for future research.

Key Points

- Introduction to hPF-MD.
- hPF-MD allows simulations of detailed models on large time and length-scales.
- OCCAM code implementation of hPF-MD.
- Open issues and perspective for future research.

1 Introduction

The first two papers about Molecular Dynamics (MD) simulations were published in 1957 by Alder and Wainwright about phase transitions in hard spheres[1] and on the methodology of MD.[2] After these two seminal papers, different efforts were devoted to model realistic molecular systems for direct quantitative comparisons with experiments. In 1964 Rahman did the first simulation of liquid argon[3] and later in 1971 Rahman and Stillinger simulated liquid water using a model consisting of 216 rigid molecules at mass density 1 g/cm^3.[4] After these very early atomistic models of liquids, several successful efforts have been made to extend the molecular simulation approaches to liquids,[5] proteins[6] and biomembranes.[7] For a complete account of the early history of molecular simulations the reader can refer to a recent book of Battimelli, Ciccotti and Greco.[8]

Nowadays atomistic simulations not only can provide good previsions and explanations for molecular mechanisms of several macroscopic phenomena, but they can be an aid to experimentalists in the interpretation of data on proteins,[9] to develop new materials[10] and to improve their production.[11] To this aim, several software packages are available to perform classical atomistic MD simulations, including GROMOS, Amber, CHARMM, GROMACS, LAMMPS, YASP and NAMD and many applications to several challenging problems have been pursued.

Computational models at atomic resolution, being the least affected by a need to effectively incorporate degrees of freedom that are disregarded, are the ideal way to face this type of problems. Unfortunately, most of the time, the length and time scales involved in relevant phenomena would require computational efforts that can be unaffordable on a routinely basis or even out of reach for actual computer power. In this respect, some typical examples are protein folding[12] and membrane remodeling.[13] For most of the proteins, atomistic modeling, due to the size of their conformational spaces, would require time scales that are still too large to be studied. Remodeling of biological membranes is particularly difficult to study because of their rich chemical composition. Moreover this problem is further complicated by membrane proteins and by dynamical structural deformations happening during biological activity, like the appearance of mesoscopic structures such as tubules, rafts, patches and undulations.[14,15]

The study of synthetic polymers can be considered the most paradigmatic example of the difficulty of modeling relevant phenomena and scales at atomistic resolution. Long chain molecules forming condensed phases of polymeric materials are intrinsically multiscale objects. Indeed, even the description of a single molecule cannot ignore strongly coupled scales ranging from the monomer (or submonomer) to the entire chain. Moreover a sharp separation of different scales determining the behavior of polymeric materials is difficult. Indeed the more local scales ranging from chemical bonds to chain conformations rearrangements are strongly coupled to mesoscale multi-chain organization and this latter is again strongly overlapped with more macroscopic scales related to mechanical properties usually described by continuum mechanics. For example, in the study of rheological properties of polymers (viscoelasticity for example), taking into account the multiscale nature of this materials is mandatory.

For this reason, the community of polymer theoreticians and simulators has been among the first one developing coarse-grained (CG) models and in general multiscale molecular simulation techniques aimed at bridging the different scales from atomic up to continuum mechanics elements. To our knowledge, earliest examples of such an effort are the OCTA project carried out in Japan at Nagoya University from 1998 to 2002,[16] BMBF Kompetenzzentrum Materialsimulation carried out in Germany from 2000 to 2005[17] (with some previous activities of the same German groups documented in Ref. 18), the development of Dissipative Particle Dynamics (DPD) simulations and relative models at Unilever.[19]

Many ways to classify CG models are possible, the resolution of the model is one criterion. Among different degrees of coarse-graining, the focus of this chapter are CG models close to atomistic resolutions. From this point of view, MARTINI,[20-22] SPICA[23,24] approaches or CG models mapped starting from reference atomistic information are the reference models.[25,26] Another criterion to classify coarse-graining approaches can be based on discrete (based on effective beads) or on continuum (based on fields for example) representations used. Particle-based CG models have been developed for real polymers (polyethylene, polycarbonates, polystyrene).[26-30] More in general, several reviews and CG models are available for this subject and the reader can refer to Refs. 31–35. Particle-based CG approaches able to represent realistic systems are still more computationally demanding than continuum models. As for continuum representations, there are mean field-based approaches in which model systems are described by density fields. This approach, for a reader familiar with methods of quantum chemistry, has many analogies with Density Functional Theory of electrons.[36] The Self Consistent Field (SCF) theory, in which mutual interactions between segments are decoupled and replaced by static external fields, is particularly popular.[37,38] External fields in SCF theories are determined by statistical averages of spatially inhomogeneous density distributions of particles generated by independent molecules interacting only with these external fields. External fields and particle density distributions must be determined in a consistent manner. SCF theory has been applied to a wide range of materials, including block copolymers, proteins, polymer composites, and colloidal particles.[37-39] SCF approaches can unquestionably access length and time scales greater than chemistry-specific CG. With these precedents, hybrid models in which particle and field coexist have been proposed as a way to solve this issue. The aim of the present chapter is to give an overview of this emerging research field with particular emphasis to developments and applications addressed to achieve chemical specific models and to provide a guide and an introduction to the hybrid particle-field MD technique (hPF-MD) for chemists, physicists, biologist and engineers in both academic and industrial environments possibly interested in applications and/or developments of this recent simulation technique. The chapter is structured in the following way: the first section is devoted to the basic theoretical background and its main results useful for the implementation of the hPF-MD simulation technique including also a short description and the references to early hybrid approaches. In this section complete derivations are not reported and the interested reader can refer to the Section 8. The second section is devoted to the description of the implementation of hPF-MD in the massively parallel code OCCAM and its parallelization strategy. Pseudo codes and strategies to turn any standard MD code into an hPF-MD one are also provided in this section. The third section is devoted to the description of some example applications to biomolecules and surfactants in water (mainly biomembranes, first subsection), polymer composites (second subsection) and all-atom models of polymer melts and glasses (third subsection). The last section, before conclusions and perspective, is devoted to more recent developments aimed to address dynamics in the hybrid models. The last section "further reading" contains a guide to books and useful papers for the reader interested in a deeper understanding of the roots of the simulation technique.

2   Hybrid Particle Field-Models: Theoretical Background

As was pointed out in the previous section, hybrid particle-field models are expected to be efficient in constructing a multi-scale representation for systems with mesoscopic structures, such as polymers and surfactant systems. One of the first hybrid particle-field approaches in this context was proposed by one of the authors of the present chapter for phase separating surfactant solutions as a model of microemulsion.[40–42] In this hybrid formulation, the phase separating binary mixture was described by a field variable using Ginzburg-Landau model while the surfactant molecules are treated as coarse-grained discrete molecules. This hybrid model was successful in reproducing the complex domain structures due to the reduction in the surface tension of surfactant-adsorbed interfaces and the decelerated coarsening in the phase separating dynamics. Similar hybrid approaches were later applied to phase separating binary mixtures containing impurity particles as fillers by Ginzburg et al.,[43–45] by Zhu and Ma,[46] and by Pinna et al.,[47] Laradji et al.[48] were the first to employ density fields, calculated on the fly, in off-lattice Monte Carlo (MC) simulations to examine the equilibrium characteristics of polymer brushes, while the mean-field technique described by Daoulas and Müller and named Single Chain in Mean Field (SCMF) MC has been the first hybrid approach introduced in the context of SCF theory.[49]

3   Hybrid Particle-Field Molecular Dynamics

This section provides an overview of the hPF-MD approach. The hPF approach considers a molecule to interact with surrounding molecules via an external field composed of non-homogeneous spatial density distributions of segments of independent molecules. The main problem with this approach is determining the partition function of a single molecule in an external field, as well as obtaining an appropriate expression for the external potential $V_K(r_i)$ and its spatial derivatives. Ref. 50 provides detailed derivations beginning with the partition function definitions. It can be shown that the density-dependent external potential can be written as functional derivative once the form of total energy is given. For example if one assumes the following functional form introduced by Helfand:[51]

$$W[\phi_K(\boldsymbol{r})] = \int d\boldsymbol{r} \left[\frac{k_B T}{2} \sum_{KK'} \chi_{KK'} \phi_K(\boldsymbol{r}) \phi_{K'}(\boldsymbol{r}) + \frac{1}{2\kappa} \left(\sum_K \phi_K(\boldsymbol{r}) - 1 \right)^2 \right], \tag{1}$$

according to saddle point approximation the external potential can be obtained as functional derivative of Eq. (1) and the potential acting on the particle can be written in the following way:

$$k_B T \sum_i \left(\sum_{K'} \chi_{KK'} \phi_{K'}(\boldsymbol{r}_i) + \frac{1}{\kappa} \left(\sum_K \phi_K(\boldsymbol{r}_i) - 1 \right) \right), \tag{2}$$

where each system component is designated by an index K. The mean field interaction parameter between a particle of type K and the density field of particles of type K' is denoted by $\chi_{KK'}$. The notation adopted for the mean field interaction parameter refers to Flory Huggins (FH) theory where χ is the adimensional mixing enthalpy.[52] Here the $\chi_{KK'}$ has a similar physical meaning, but the density is a field and, differently from FH theory, the interaction is with a local density at a position r. The density field of the species K at location r is given by $\phi_K(r)$, and κ is the compressibility term. This term is a penalty function introduced by Helfand, which penalizes differences with a constant (background) value. In other words, if in a given region of the space there are too many or too few particles this term gives rise to repulsive or to attractive forces, respectively. The Boltzmann constant is denoted by k_B, while the system temperature is denoted by T. The mean field potential in the basic situation of a two component mixture, A and B, of a single particle of type A at location r is:

$$V_A(\boldsymbol{r}) = k_B T [\chi_{AA} \phi_A(\boldsymbol{r}) + \chi_{AB} \phi_B(\boldsymbol{r})] + \frac{1}{\kappa} (\phi_A(\boldsymbol{r}) + \phi_B(\boldsymbol{r}) - 1). \tag{3}$$

To be more specific about parameters, in the case of a hydrophobic particle type A in water (type B), the χ_{AB} would be large and positive. Differently, for a hydrophilic particle χ_{AB} would be positive small or negative. The incompressibility condition keeps the density homogeneous in the space and represents the excluded-volume interaction in traditional molecular dynamics simulations based on pair potentials.

Then, the force acting on particle A at position r is:

$$F_A(\boldsymbol{r}) = -\frac{\partial V_A(\boldsymbol{r})}{\partial \boldsymbol{r}} = -k_B T \left(\chi_{AA} \frac{\partial \phi_A(\boldsymbol{r})}{\partial \boldsymbol{r}} + \chi_{AB} \frac{\partial \phi_B(\boldsymbol{r})}{\partial \boldsymbol{r}} \right) - \frac{1}{\kappa} \left(\frac{\partial \phi_A(\boldsymbol{r})}{\partial \boldsymbol{r}} + \frac{\partial \phi_B(\boldsymbol{r})}{\partial \boldsymbol{r}} \right) \tag{4}$$

We would like to stress that, obviously, different functional forms of Eq. (1) would lead to different forms of the expression of external potential and in turn of the force acting on particles. As will be shown later, from this point of view, the scheme handling hPF-MD simulation is general and does not change if different functionals are adopted. We suggest, in strict analogy with classical MD simulations, in order to avoid confusion in the audience, the functional form of intramolecular (bond, angle, dihedral terms) and of the non-bonded potentials (energy functional for hPF and pair potential for traditional MD), together with corresponding parameters, constitutes a hybrid force field for a given molecular system. It is worth noting that intra-molecular terms do not depend on the field, and can be therefore simply adopted from the particle-based CG model that one considers. This is one of the main advantages of hPF simulations in comparison with pure field models based on SCF theory. Indeed, in hPF-MD simulations any kind of complex chemical structures or complicated functional forms of intramolecular interactions, differently from SCF theory, can be

adopted. For example, using hPF-MD, combined potentials for the bending and the dihedral angle able to achieve models showing secondary structure elements of polypeptides together with a field description of non-bonded interactions have been proposed.[53]

3.1   Electrostatic Interactions in the hPF Approach

The approach described in this section has been originally developed in Ref. 54 and the reader can refer to this paper for more complete information. The electrostatic interactions between charged particles are evaluated through an electric field E-field which depends on the spatially inhomogeneous distributions of charge densities.[7,9] The E-field can be represented by dividing the simulation box (L_1, L_2, L_3) into $N_1 \times N_2 \times N_3$ cells (the $N_\alpha =$ number of cells in the direction L_α for $\alpha = 1, 2, 3$). The location of lattice points is given by $l = l_1 L_1/N_1, l_2 L_2/N_2, l_3 L_3/N_3$, where l_α is an integer number $0 \leq l_\alpha < N_\alpha$ The total Coulomb energy can be written as:

$$E = \frac{1}{2}\sum_i q_i \psi(r_i), \tag{5}$$

where q_i is the reduced charge of the i-th particle and $\psi(r)$ is the electrostatic potential. Collecting the contribution over i-th particles gives $\psi(r)$:

$$\psi(r) = k_b T l_B \sum_n \sum_j \frac{q_j}{|r - r_j + n|} \tag{6}$$

The outer sum over n is, with periodic boundary conditions, over the vectors $n = n_1 L_1 + n_2 L_2 + n_3 L_3$. The Bjerrum length is $l_B = \frac{e^2}{4\pi\epsilon_0 \epsilon_r k_B T}$, where e is the elementary charge and ϵ_0, ϵ_r are the vacuum permittivity, and the relative dielectric constant of the medium. $\psi(r)$ can be separated in long and short range contributions by using the Ewald summation:

$$\psi^S(r) = k_B T l_B \sum_n \sum_j \frac{q_j erfc(\alpha|r - r_j + n|)}{|r - r_j + n|}, \tag{7}$$

$$\psi^L(r) = \sum_{m \neq 0} \hat{\psi}^L(m) exp(im \cdot r). \tag{8}$$

The term $\hat{\psi}^L$ on the right hand of Eq. (8) is the long-range contribution of the electrostatic potential in the reciprocal space. It is feasible to solve the Poisson's equation in the reciprocal space using the Gaussian distribution of charge density and obtain $\hat{\psi}^L(m)$:

$$\hat{\psi}^L(m) = \frac{4\pi k_B T l_B exp\left(-\frac{m^2}{4\alpha^2}\right)}{V m^2} \sum_{j=1}^N q_j exp\left(-im \cdot r_{J+j}\right) \tag{9},$$

where V is the box volume and $m = 2\pi(m_1 L_1^* + m_2 L_2^* + m_1 L_1^*)$. The L_α^* are the conjugated reciprocal vectors defined by the relations $L_\alpha^* \cdot L_\beta = \delta_{\alpha\beta}; \alpha, \beta = 1, 2, 3$.

Using the discrete Fourier transform (DFT), the long-range contribution of the electrostatic potential at the lattice point of special location L may be represented as follows:

$$\psi^L(l) = \sum_{m \neq 0} \hat{\psi}^L(m) exp(im \cdot l) = \sum_{m_1=0}^{N_1-1} \sum_{m_2=0}^{N_2-1} \sum_{m_3=0}^{N_3-1} \hat{\psi}^L(m)\left[2\pi i\left(\frac{m_1 l_1}{N_1} + \frac{m_2 l_2}{N_2} + \frac{m_3 l_3}{N_3}\right)\right] = F^{-1}[CF(Q)](l_1, l_2, l_3), \tag{10}$$

where Q is the charge density at lattice points, and $F(Q)$ is the DFT, and F^{-1} is the inverse DFT.

Because only mean field parameters are applicable in the hPF technique, short-range electrostatic interactions, which are normally regarded pairwise interactions in traditional MD, can be assessed as follows. It is feasible to assess a χ_e parameter for the short-range component of electrostatic interaction in analogy to the Flory-Huggins approach for lattice models:

$$\chi_e = \frac{z}{k_B T}\left[2u_{CC'} - \frac{u_{CN} + u_{C'N}}{2}\right] = \frac{z l_B erfc(\alpha\sigma)}{\sigma} \tag{11}$$

where z is the coordination number ($z = 6$ for a 3D cubic lattice), while $u_{CC'}, u_{CN}, u_{C'N}$ are the pairwise short-range electrostatic energies between a pair of adjacent lattice sites ($u_{CC'} = k_B T l_B ercf(\alpha\sigma)/\sigma$). σ is related to the diameter of particles. The terms $u_{CN} = u_{C'N} = 0$ for lattice sites occupied by one particle with (e) and other one being neutral. The short-range part of the electrostatic potential $\psi^S(l)$ can be obtained in the density field fashion:[5]

$$\psi^S(l) = \chi_e Q(l_1, l_2, l_3) k_B T. \tag{12}$$

3.2   Pressure Calculation

The calculation of pressure is an important ingredient for several applications of MD simulations. The evaluation of stress tensor for a hybrid particle–field Hamiltonian is not a trivial task. The general formulation for the calculation of instantaneous pressure and the stress tensor in hPF-MD simulations has been proposed in Ref. 55 and is summarized later in this section. For similar hybrid models, other strategies for the pressure calculation and for isothermal isobaric simulations have been also proposed. In particular, Kremer and Daoulas implemented a 'volume-changing' move used in isothermal isobaric (NPT) simulations of standard potential-based models.[56] Constant pressure simulations have been implemented for hybrid particle-field models by using Field-accelerated Monte Carlo[57] and hPF-MD simulations.[58]

The intramolecular terms (bonds, angles, etc.) will not be treated here because standard virial approaches are applied to them as in traditional MD simulations. Here we report the scheme developed in Ref. 55 and applied to the energy functional corresponding to Eq. (1). The same derivation scheme can be applied to different hybrid molecular force-fields corresponding to different energy functionals. In particular, starting from the expression of the free energy functional obtained using the SCF theory for a system of M molecules (for simplicity we consider just one species):

$$F[\phi(\mathbf{r})] = -k_B T ln z^M + W[\phi(\mathbf{r})] - \int d\mathbf{r} V(\mathbf{r})\phi(\mathbf{r}) + k_B TM(ln M - 1), \tag{13}$$

Let's suppose we are deforming the box by multiplying all the components of the particle positions by a factor λ. This is a simple example of a uniform transformation

$$\begin{cases} x' = \lambda x \\ y' = \lambda y \\ z' = \lambda z \end{cases}. \tag{14}$$

For example, for the first coordinate $x' = x + u(x)$ which means $u(x) = \lambda x - x$. If the deformation is a function of the position, the Jacobian for the transformation will be

$$det \begin{pmatrix} 1 + \dfrac{\partial u}{\partial x} & 0 & 0 \\ 0 & 1 + \dfrac{\partial u}{\partial y} & 0 \\ 0 & 0 & 1 + \dfrac{\partial u}{\partial z} \end{pmatrix}. \tag{15}$$

In this way, the change in the volume element will be $d\mathbf{r}' = d\mathbf{r}(1 + \nabla \cdot \mathbf{u})$. This factor is a Jacobian of the transformation which should be a scalar quantity. This means that a scalar quantity $A(r)$ that has the dimension of density should be transformed as $A'd\mathbf{r}' = Ad\mathbf{r}$ due to the conservation of material, which leads to $A' = A|\frac{d\mathbf{r}}{d\mathbf{r}'}|$. The factor $|\frac{d\mathbf{r}}{d\mathbf{r}'}|$ is the inverse of the Jacobian $(1 + \nabla \cdot \mathbf{u})^{-1} \sim (1 - \nabla \cdot \mathbf{u})$.

In order to calculate the pressure tensor, we consider a virtual displacement $\mathbf{r}' = \mathbf{r} + \mathbf{u}(\mathbf{r})$, which leads to a change in the area element $d\mathbf{r}' = d\mathbf{r}(1 + \nabla \cdot \mathbf{u})$. Then we have the following expressions for ϕ and V in the transformed coordinates $\mathbf{r}'$

$$\phi'\left(\mathbf{r}'\right) = \phi(\mathbf{r}) - \phi(\mathbf{r})(\nabla \cdot \mathbf{u}), \tag{16a}$$

$$V'\left(\mathbf{r}'\right) = V(\mathbf{r}) - V(\mathbf{r})(\nabla \cdot \mathbf{u}), \tag{16b}$$

Using these transformations, we can then calculate the pressure from free energy increase after deformation for the first three terms of Eq. (13). For the complete derivation the reader can refer to Ref. 55. Here we report the final result including also the term due to electrostatic interactions:

$$\Pi_{\alpha\beta} = \Big\{ -M \, k_B \, T \langle \big(1 + \beta \sum_i V\,(\mathbf{r}_i) \big) \rangle$$

$$- k_B \, T \frac{1}{2V} \Big[\sum_{KK'} \chi_{KK'} \int d\mathbf{r} \phi_K(\mathbf{r})\phi_{K'}(\mathbf{r}) \Big]$$
$$+ \frac{1}{2\kappa V} \Big[\int d\mathbf{r} \big(1 - \sum_K \phi(\mathbf{r}) \big)^2 \Big]$$
$$+ \Big[\frac{1}{V} \sum_K \int d\mathbf{r} \phi_K(\mathbf{r})V_K(\mathbf{r}) \Big]$$
$$- \frac{1}{2} \Big[\sum_i q_i \psi(\mathbf{r}_i) \Big] \Big\} \frac{1}{3} \delta_{\alpha\beta} \tag{17}$$

3.3 Different ("Non-Helfand") Functionals

The functional of Eq. (1), which combines a cohesive energy term in the spirit of mean-field Flory-Huggins theory with an excluded-volume term introduced by Helfand[51] for imposing the weak compressibility of liquids, can be seen as the non-ideal part of the free energy in self-consistent field theory for (block co-)polymer liquids. Indeed, simple and complex liquids deviate from most other phases by the fact that they are mildly compressible (the isothermal compressibility of water is finite). The key challenge in hPF-MD is in the mapping of non-bonded interactions of the pure particle-based description, at the desired atomistic or coarse level of resolution, into representative values of the mean-field Flory interaction parameters $\chi_{KK'}$ and Helfand parameter κ in hPF-MD. In reality, determining Flory parameters is the only challenge. The aim here is to capture all particle-particle (two-body) interactions in an effective mean-field strength between each particle and all concentration fields. The value of κ can be matched only once via the equations of state (EOS) for the pressure of a single particle type system in both descriptions.[59] However, the EOS route is often deemed unnecessary, and it is common practice to base the choice of κ on considerations about the permitted/reference (small) amplitude of fluctuations around the (fixed) total fluid density.

Owing to the quadratic nature of the excluded volume term of Helfand used in (1), which penalises any deviation of the total density from a fixed value anywhere in the volume and gives rise to a quadratic EOS for the pressure that lacks a so-called van der Waal loop, this functional is not suited for phenomena that involve a pressure (or total density) difference over the simulation volume. Key examples of interest to the soft matter community include the solvent evaporation that takes place upon thermal annealing of spin-coated block copolymer films, which can strongly affect orientational order, and the phase transition/coexistence between gel (liquid ordered) and fluid (liquid disordered) phases in (mixed) lipid membranes. In order to enable hPF-MD also to capture phase coex-istences, the incorporation of higher order terms in the corresponding EOS is essential.[60] This issue was previously identified and addressed, albeit that application is somewhat limited due to additional parametrization required. A particle-based method known as multi- or many-body DPD or DPD[61–63] introduces density-dependent soft two-body interaction potentials to arrive at the desired higher-order EOS. Two excluded-volume terms introduced for compressible SCF,[64] one based on the familiar Carnahan-Starling (CS) expression for hard spheres,[65] have been adopted to arrive at a hPF-MD for two-phase systems (coined c-hPF-MD). Introducing a more general excluded-volume term in the functional (1), and concentrating on CS and a single particle-type - we refer to the original paper for more detail - the contribution of the excluded-volume in the external potential (2) is replaced by

$$\frac{V^e(r)}{k_bT} = \frac{\eta(4 - 3\eta)}{(1 - \eta)^2} + \frac{4\eta - 2\eta^2}{(1 - \eta)^3} \tag{18}$$

with $\eta = \eta(r) = v\rho(r)$ and v the volume of the particle. Defining a dimensionless interaction parameter $\tilde{\chi} = \chi/k_BTv$, we can now write the total force on each particle as

$$\frac{F(r)}{k_BT} = -\left[\tilde{\chi} + \frac{2(\eta(r) - 4)}{(1 - \eta(r))^4}\right]\nabla\eta(r), \tag{19}$$

which replaces the original force expression (4) of hPF-MD based on (1). We note that, in the original hPF-MD, the cohesive interaction for a single-particle system vanishes ($\chi = 0$) by definition, leading to the situation were particles are homogeneously dispersed over the simulation volume due to excluded volume repulsions, while the same system in c-hPF-MD will be also homogeneous for $\tilde{\chi} = 0$, but it will phase separate into a coexisting gas and liquid domain for $\tilde{\chi} < \tilde{\chi}_c$, with $\tilde{\chi}_c = 21,2024541158$ as determined from mean-field theory.[60] In particular, the attraction due to a negative $\tilde{\chi}$ balances the density-dependent repulsion due to CS term. For background information, validation to analytic mean-field results, and basic examples, we refer to the published study.[60] An interesting observation is the finding of a critical exponent for c-hPF-MD that deviates from the theoretical mean-field value of 0.5, despite the clear mean-field origin of hPF-MD. We note that incorporating other EOS are a viable option, and that, while the Flory interaction strength is temperature dependent, the cohesive energy part of the functional (1) is not changed in c-hPF-MD (Fig. 1).
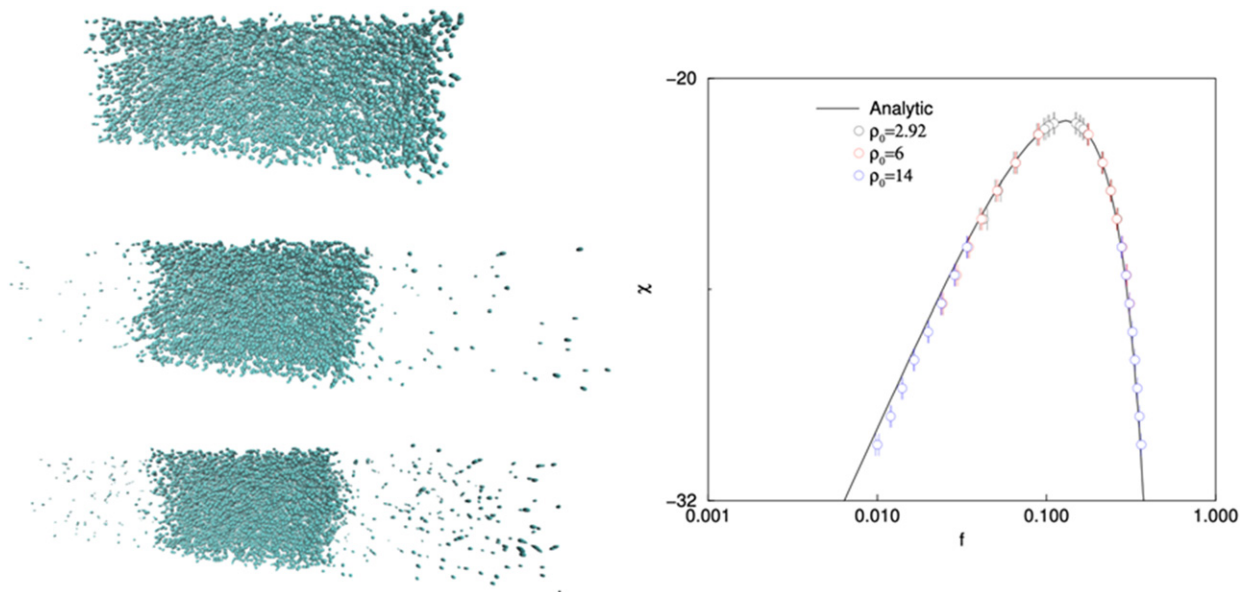
Fig. 1   (left) Illustrative snapshots of a single-bead system at different stages along the systems evolution, from the mixed starting structure (top), phase separating intermediate (middle) and stable coexistent gas-liquid end (bottom) stage. The overall number density that sets the total number of particles in the simulation volume is $\rho_0 = 2.92$ for this particular setup. (right). Phase diagram of a simple liquid. Reproduced from Sevink, G.J.A., Blokhuis, E.M., Li, X., Milano, G., 2020. Efficient and realistic simulation of phase coexistence. Journal of Chemical Physics 153 (24). https://doi.org/10.1063/5.0027778.

Fig. 2 (A) The iteration scheme hPF-MD simulation and the relative pseudocode; (B) Scheme for particles assignment to lattice points (2D simplified example). Fractions assigned are proportional to the area of a rectangle whose diagonal is the line connecting the particle position and the mesh point on the opposite side of the cell (empty crosses indicate the staggered lattice where the derivatives are defined) and 3D scheme of the gradient directions around a 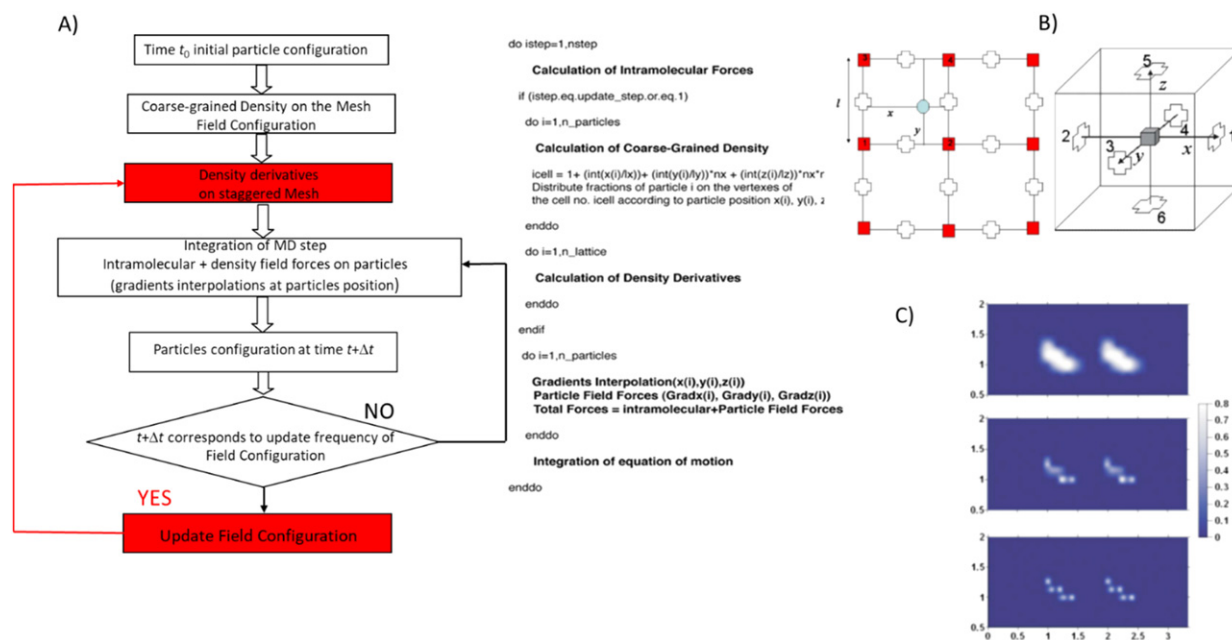given lattice point; (C) 2D density maps corresponding to a test configuration containing two n-pentane molecules at different grid resolutions (from the top l = 0.166, 0.083, and 0.066 nm). Panels (B) and (C) reproduced from J. Chem. Phys. 130, 214106, 2009. https://doi.org/10.1063/1.3142103.

4   Implementation of hPF-MD: The OCCAM Code

A strategy for obtaining a smooth coarse-grained density function from particle locations is required to link particle and field models. **Fig. 2**A depicts the iteration scheme utilized in the hPF-MD and the corresponding Fortran pseudocode. The initial setup of the system at time t_0 yields the starting value of the density dependent external potential. The forces acting on the particle come from the total intramolecular interaction terms such as bonds, angles, dihedrals, and so on, as well as density dependent interactions. Integrating the equation of motion of the particles from time t_0 to time $t_0 + \Delta t$ yields a new configuration. The density is calculated according to the updated particle locations at each predetermined density update period. The new density value is used to produce a new external potential, which is subsequently used to compute new forces from density spatial derivatives. The central part of a code doing hPF-MD simulations is the calculation of density fields (i.e., the value of the number density of the different particle types as function of the position in the three-dimensional space) and their spatial derivatives in the Cartesian directions.

An effective approach to have these quantities is to define them on a grid of a given resolution. To calculate coarse-grained density, the simulation box is divided into cells. According to their positions in the simulation box, all the particles are distributed among these cells. In the implementation of OCCAM, the cells data structure can be implemented using the method of "linked lists" that assures a rapid sorting of the particles.[66] In this way density fields and their derivatives are used for the calculation of the forces and they are both defined on three-dimensional lattice points obeying the periodic boundary conditions. The values of the density field at position r between lattice points are evaluated using linear interpolation of the values at neighbor lattice points. To calculate the density field values on the mesh at each update, fractions of a particle are assigned to its neighbor mesh points according to the distances from the particle to the mesh points as explained in **Fig. 2**(B). In **Fig. 2**(C), we show three two-dimensional density maps corresponding to a test configuration containing two n-pentane molecules in all trans conformation lying in the xy plane at different grid resolutions starting from the top l = 1.66, 0.83, and 0.66 Å.

The spatial derivatives of the density distribution are specified on a staggered lattice, as shown in **Fig. 2**(B). The density field computation is accomplished, as shown in **Fig. 2**(A), by looping over the number of particles N to compute the coarse-grained density on the vertexes of the cells where the density field is specified. Density derivatives on the staggered lattice are computed by looping over the number of lattice points $n_{lattice}$. In terms of computing efficiency, the hybrid hPF-MD technique provides a significant advantage over traditional MD simulations. The most computationally expensive element of the MD simulations, namely the evaluation of inter-molecular non-bonded forces and the relative neighbor lists (or similar), is totally replaced by an evaluation of particle-field forces coming from individual particle interactions with density fields. This implies that at each time step, the double loop over particle pairs used in standard MD simulations to calculate non-bonded forces is replaced with a single loop over N particles used to interpolate
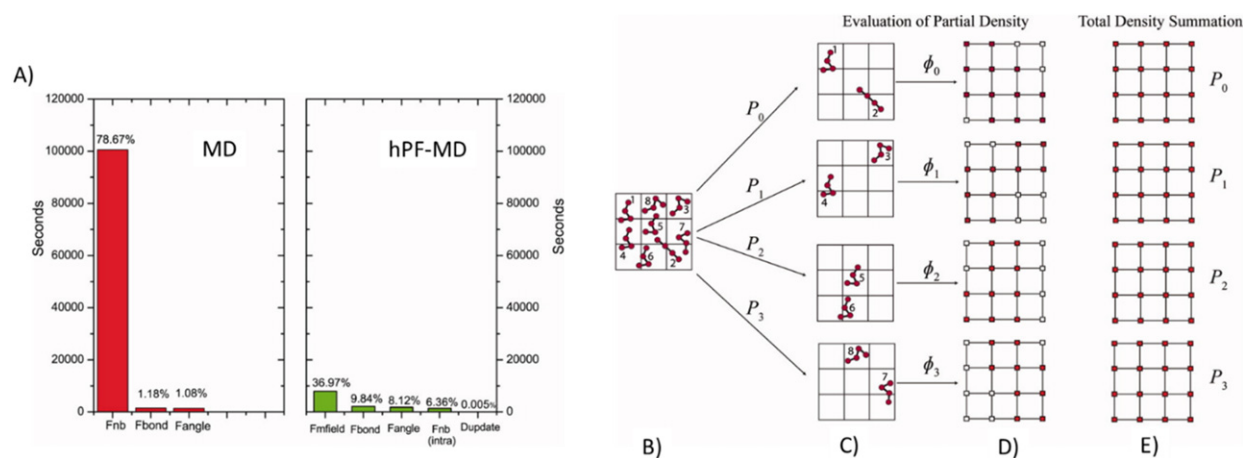
Fig. 3 (A) Serial MD and hPF-MD OCCAM code profiles obtained by gprof v2.17 in reference Zhao, Y., De Nicola, A., Kawakatsu, T., Milano, G., 2012. Hybrid particle-field molecular dynamics simulations: parallelization and benchmarks. Journal of Computational Chemistry 33 (8), 868–880. https://doi.org/10.1002/jcc.22883; (B–E) Simplified scheme of the parallelization strategy adopted in OCCAM.

density gradients (for each particle type) at particle locations. Following the computation of the force, a new configuration will be obtained by integrating the equation of motion. In principle, for each new configuration, the coarse-grained density estimated from the new coordinates should be updated. Because of the collective character of the density fields, an update frequency of the coarse-grained densities may be defined, given the kinetic model (this issue is discussed later in the section about dynamics), without sacrificing accuracy.[49] In other words, the coarse-grained density values at lattice points are not updated at each timestep, but can only be computed at each predetermined density-update time. This approximation in the context of SCMF MC simulations has been named by Daoulas and Müller "*quasi instantaneous field approximation*".[49] The values of the densities on the lattice used to interpolate both density and its derivatives during the particle movements at each timestep will then be unchanged between two updates.

Fig. 3(A) makes it evident that the most time-consuming part of serial MD simulations, which accounts for over 80% of total simulation time, is the computation of non-bonded forces. Non-bonded forces cost is around 70 times more expensive than bond forces and angle forces. Nevertheless, in hPF-MD simulations, forces between individual particles and the density field are calculated in place of the costly intermolecular non-bonded forces. As a result, the overall duration of hPF-MD simulation is drastically reduced. Hence, for example for the tests reported in Ref. 66, although the corresponding serial hPF-MD simulations only take about 21 s, the serial MD simulation takes about 128 s (about six times slower than hPF-MD simulation). Moreover, the serial hPF-MD simulation differs from serial MD in that it has a flat profile. The interpolation of density and density gradients (which takes up 37% of the overall simulation time) and the computation of intramolecular interactions (which takes up around 18% of the total simulation time) are the two most time-consuming and expensive steps in the serial hPF-MD simulation. In the end, the computation of density derivatives and the density-update from the particle locations only account for a tiny fraction (0.005%) of the whole simulation.

The hPF-MD technique is very suitable to be efficiently parallelized. Below the main information about an efficient parallelization of hPF-MD simulations are given.

In Fig. 3(B–E), the parallelization strategy is schematically depicted. In particular, N particles belonging to M molecules are assigned to P processors in accordance with the molecular decomposition criterion. Strictly speaking molecules, independently from their spatial positions are assigned to a given processor. As a result, N/P particles are owned by each processor during the hPF-MD simulations. It is important to remember that a molecule's constituent particles are all allocated to the same processor. Therefore, N_{bonds}/P, N_{angles}/P, and $N_{dihedrals}/P$, etc. respectively, are the amounts needed to calculate the intramolecular interaction forces (bonds, angles) (as shown in Fig. 3C). As previously mentioned, the calculation of forces acting on each particle owing to density field takes the role of the traditional MD simulations' calculations of intermolecular non-bonded forces. Eqs. (2) and (4) state that the relative forces and potential energy of particle-field interactions may be determined from particle locations by interpolating the values of the density fields and their spatial derivatives. Moreover, rather than being derived from particle locations at each time step, the density field (and its derivatives) are updated at lattice points only at a predetermined frequency. This implies that the computation of potential energy and forces acting on the particles may be totally parallelized between two density updates and does not entail any processor communication.

The density on the lattice points is assessed at the beginning of the simulation and then at each subsequent update time, Δt_{update}. In the parallelized simulation, densities are evaluated for each processor's individually only from the molecules owned by a given processor. The total coarse-grained density on the lattice points is then obtained by performing an MPI_ALLREDUCE call with the MPI_SUM operator and adding the partial densities held by each processor. Fig. 3(B) illustrates the parallelization strategy for the communication operation to acquire the total density and the assessment of partial density. In the Fig. 3(B) an eight-molecule system in a concurrent simulation running on four CPUs is depicted as an example. Initially, there are four groups of eight molecules in Fig. 3(C), each of which is allocated to one of the four processors. The two molecules that each processor possesses (as shown in Fig. 3C), for instance, processor P_0 is the

Vertical: Information is mapped from Atomistic to Mesoscale Models and Back
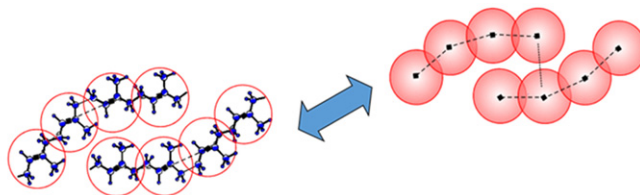
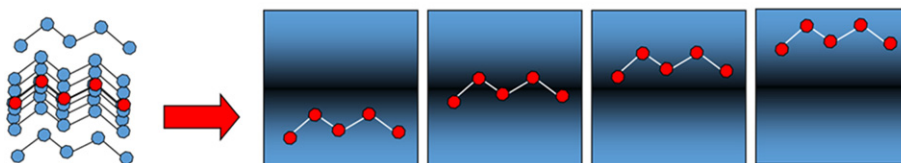Horizontal: Two Scales Co-exist

Fig. 4 Comparison of vertical and horizontal approaches in coarse-graining. The lower panel depicts the hPF approach where intramolecular interactions are treated as in traditional MD models, while non-bonded interactions are described by density fields.

owner of molecules 1 and 2, and ϕ_0 represents the partial density field computed using only the atom locations of these two molecules owned by P_0. The partial densities fields of molecules held by processors P_1 to P_3 are similarly indicated by ϕ_1 and ϕ_3. To obtain the total coarse-grained density, each processor must then expand the coarse-grained partial density over all processors and add it. The complete number of lattice points are communicated with this operation in an all-to-all manner. It is important to note that in ordinary applications, cells typically contain one to ten particles.[67] This indicates that the coarse-grained density cell size may often be 30 times smaller than the size of the particle coordinates. We emphasize that the presented scheme fully parallelizes the computation of partial density, and that, in contrast to traditional MD simulations, particle coordinates are never shared between multiple processors; only the density fields are shared. We would like to emphasize that domain decomposition schemes would be not useful in hPF-MD simulations. Indeed, sharing parts of a given molecule on different processors would cause the communication of particle positions (at each timestep) only for the calculation of bonded terms causing a fatal decrease of code performances.

hPF-MD is also suited to exploit Graphic Processing Units (GPU) and an efficient implementation has been included in the GALAMOST simulation software.[68] To have a quantitative idea, from the test reported in Ref. 68 the performances of GALAMOST in hPF-MD simulations measured on GeForce GTX 580 correspond to 96 CPUs (Intel E7330, 2.4 GHz). The GPU approach can be extended efficiently for hybrid models to distributed architectures. Recently, Schneider and Müller using multi GPU architectures with SOft coarse grained Monte-Carlo Acceleration (SOMA) software implementing SCMF MC have been able to simulate large system sizes with up to billions of particles.[69]

5   Applications

Before describing the different applications of hPF-MD, it is important to clarify some concepts related to coarse-graining and in what sense (or senses) hPF-MD is a coarse-graining technique. In **Fig. 4** a schematization of two different types of coarse-graining strategies is depicted. In particular, on the top a coarse-graining approach specifically defined as vertical is depicted, where information is mapped from an atomistic level (or from a less coarse representation) to a coarser level: example of these coarse-graining schemes are Reverse Monte Carlo[70] or Iterative Boltzmann Inversion (IBI) approaches.[25] In the reverse direction, the procedure typically depends on the specific chemical structure that needs to be defined.[29,71–74] A similar scheme could also describe the parametrization of a classical force-field from a quantum chemical calculation. The second example is a horizontal coarse-graining method, in which two different representations of the same system coexist, like in hPF models. A similar horizontal approach is adopted, for example, in QM/MM simulations (where the same system is partitioned in two regions, one described quantum-mechanically and one classically).[75] Or, more similarly, the Hartree–Fock method for polyelectronic atoms also named as electronic self-consistent field approach where a single electron is described as interacting with the mean field of the remaining ones.[76]

According to the formulation of hPF-MD, in contrast to SCF theory, intramolecular bonded interactions of any type of complexity can be directly imported from force-field employed in classical MD simulations. For this reason, complex molecular representations can be treated using hPF-MD in a straightforward manner. All-atom models or CG models close to an atomic description can be readily translated in their hPF counterparts. The adoption of CG models from MARTINI force-field[22,67,77] or CG models derived from IBI[78,79] in the hPF scheme resulted in a beneficial combination of the vertical and horizontal CG approaches. The aim of this combination is to achieve models having detailed chemical features, but, at the same time, able to efficiently sample the emergence of mesoscale structures. According to this view the following test applications have been selected:
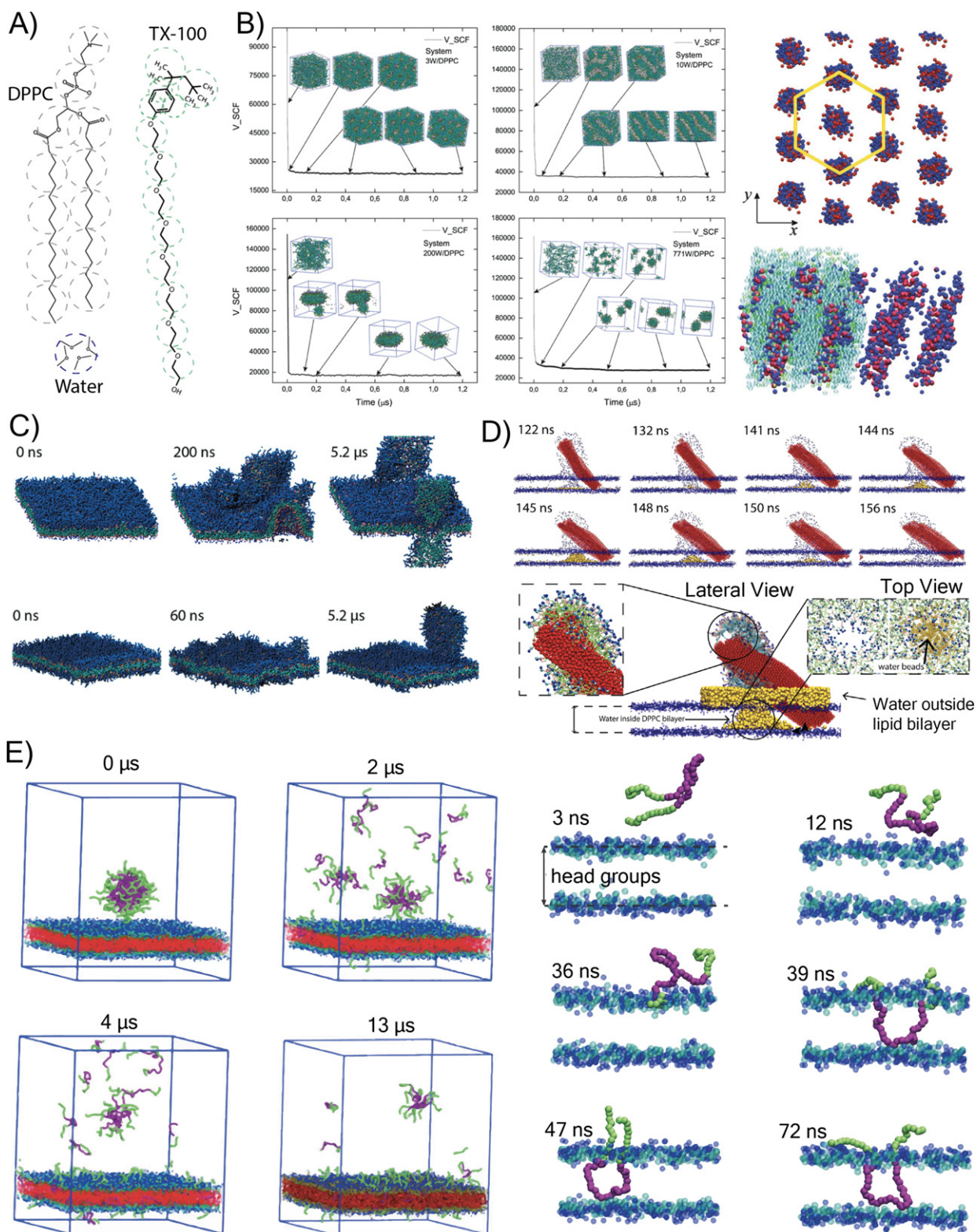
Fig. 5 (A) Mapping scheme adopted for DPPC, water and TX100 according to MARTINI; (B) Self-assembly of DPPC lipids at different water concentrations; (C) Snapshots of hPF-MD simulations of a model biomembrane solubilization process in the presence of TX100; (D) Mechanism of poration of a biomembrane in the presence of a CNT bundle observed in hPF-MD simulation; (E) Mechanism of interaction of a micelle of Pluronic containing a hydrophobic drug (left panel); Insertion of a Pluronic block copolymer inside a lipid bilayer in hairpin conformation. Panels (A), (B) reproduced from: Theor. Chem. Acc., 131:1167, 2012. https://doi.org/10.1007/s00214-012-1167-1. Panel C from: Phys. Chem. Chem. Phys., 2017, 19, 29780-29794. https://doi.org/10.1039/C7CP03871B. Panel D from: Chemical Physics Letters, 595-596, 156-166, 2014. https://doi.org/10.1016/j.cplett.2014.01.057. Panel E: Phys. Chem. Chem. Phys, 2014, 16, 5093. https://doi.org/10.1039/c3cp54242d.

Fig. 6   (A) Chain conformations of a polyelectrolyte in solution at relative dielectric constants of 3.9, 20.0, 78.0 (upper panel from left to right); Radius of gyration of the polyelectrolyte chain as function of relative dielectr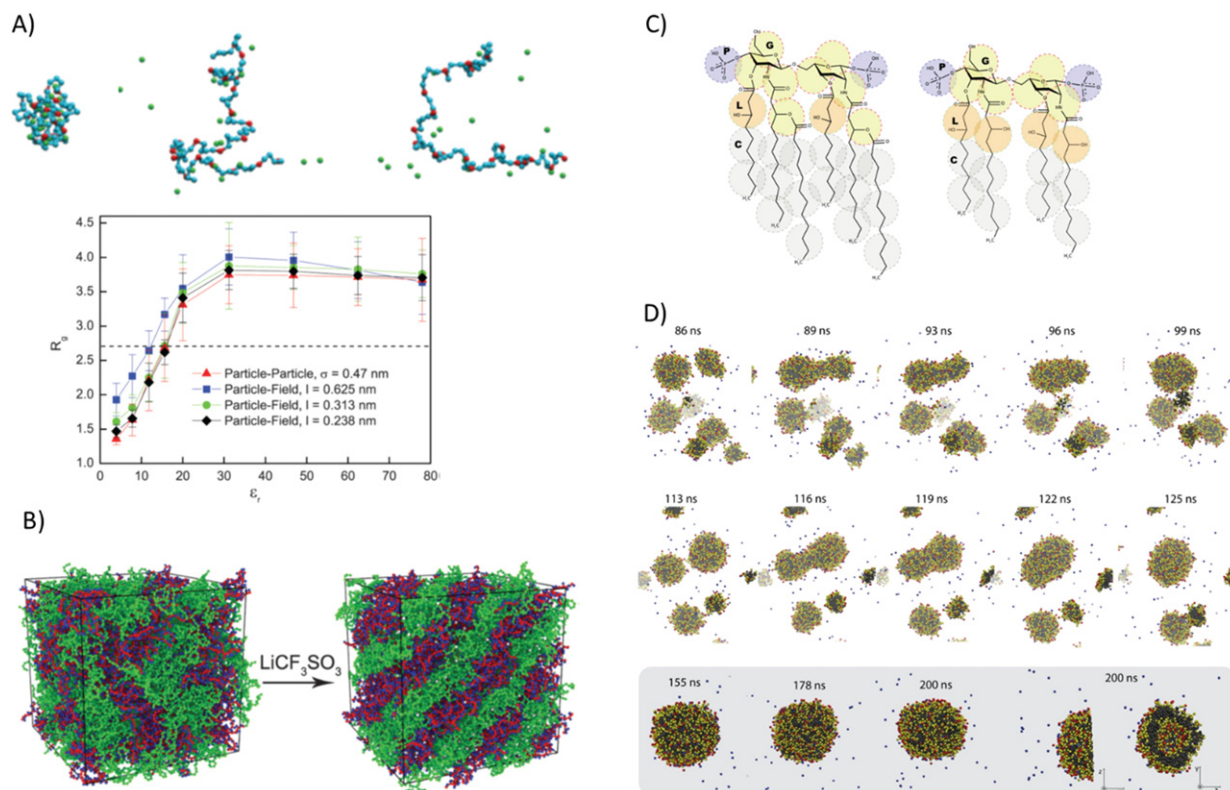ic constant for different grid resolutions; (B) Snapshots of neat (left) and salt-doped (right) PMMA-b-PEO block copolymer CG models; (C) Mapping schemes for two different variants of Lipid A; (D) Time evolution of the assembly of Lipid A molecules, a spontaneous of a vesicle by fusion of smaller micelles is observed in the last stages of the hPF-MD simulation. Panels (A),(B) reproduced from: Phys. Chem. Chem. Phys 2016, 18, 9799-9808. https://doi.org/10.1039/C5CP06856H. Panels (C),(D) from: BBA General Subjects 1865 (2021), 129570. https://doi.org/10.1016/j.bbagen.2020.129570.

(1)   Surfactants in water: phospholipids, models of biological membranes and their interactions with nanosized objects, synthetic surfactants with complex architectures, charged bacterial lipids having complex architectures (gram negative bacteria);

(2)   Polymer Nanocomposites: large scale CG models of Carbon Nanotubes (CNT) dispersed in polymer melts, silica nano-particles dispersed in polystyrene;

Moreover all-atom models of polymer melts of large molecular weights have been also considered to give an example application of hPF-MD on atomic scale. In the following sections these three different types of applications are reviewed.

5.1   Biomolecules and Surfactants in Water Solutions, Lipid Bilayers and Self-Assembled Structures

Surfactants provide a number of difficulties from the perspective of simulation because, particularly for biosurfactants, a precise representation of the complex ensemble of interactions occurring in the self-assembling processes at the molecular level is required.[80] Moreover, if the surfactants are charged, the long-ranged nature of electrostatic interactions creates additional difficulties.[81]

Phospholipids exhibit a vast variety of phases at different water compositions. They can yield diluted micellar phases as well as non-lamellar phases like the hexagonal and cubic phases. Tubular aggregates, hexagonal phases can be made up of either normal or reverse aggregates. Curved bilayers or micelles make up cubic phases. Lipids can aggregate as regular ('oil in water') or reverse ('water in oil') micelles, depending on the amount of water present. Test simulations have demonstrated the model's aptitude for accurately reproducing non-lamellar phases. Particularly, particle-field models are capable of accurately describing the many morphologies that are found experimentally, such as micelles and reverse micelles, by changing the water content. The results obtained in Ref. 77 are summarized in Fig. 5. In Fig. 5(A) the mapping scheme of DPPC phospholipid and Triton X-100 (discussed later) CG models is shown. In Fig. 5(B) snapshots of the spontaneous formation of reverse micelles, lipid bilayers, bicelles, and micelles transitions from a low to high water content are reported. In the same figure, the hexagonal packing of tubular aggregates for the system at reduced water content are also reported. We want to emphasize that while all the CG beads are included in the models, they are not implicit solvent models, since the
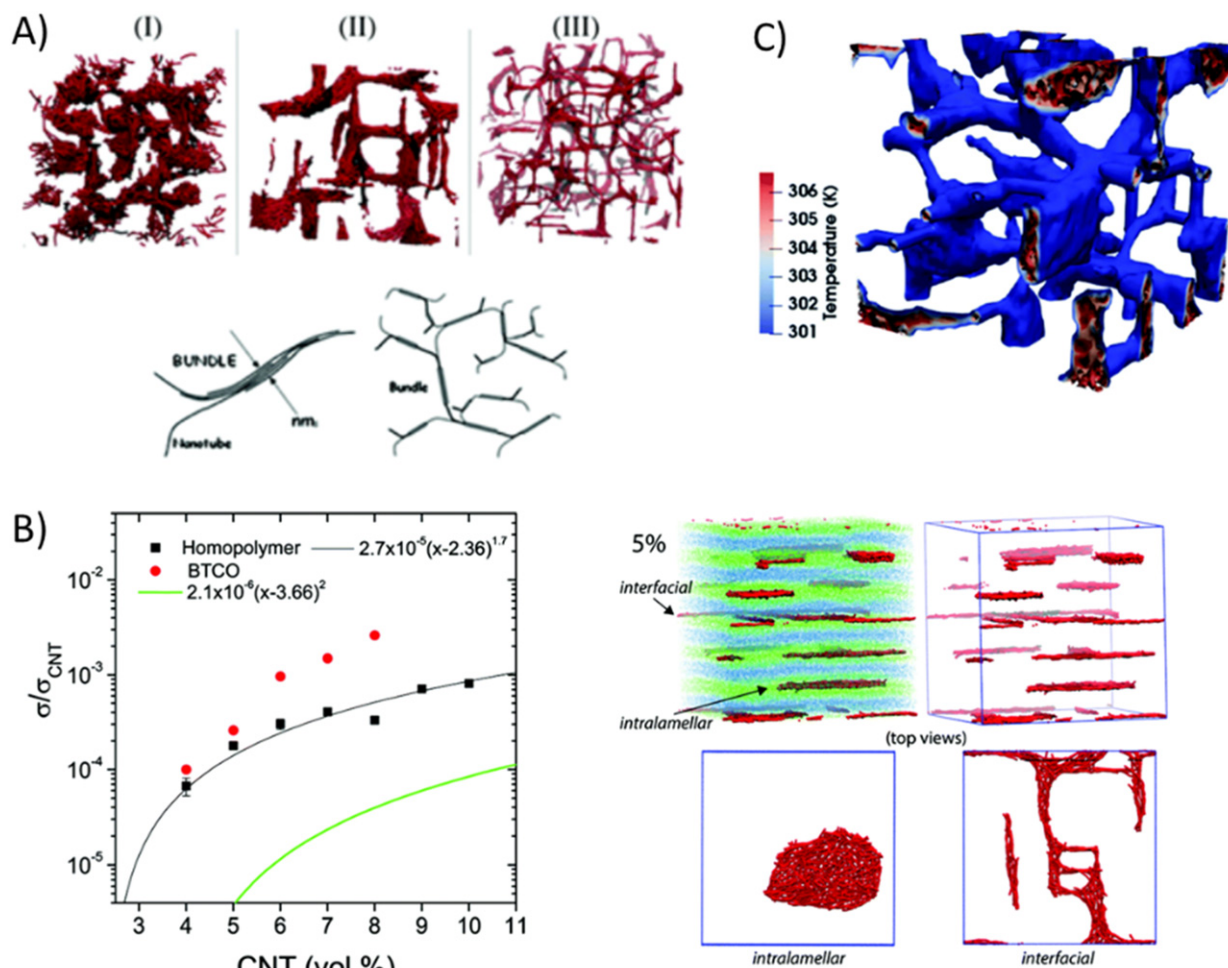
Fig. 7 (A) Snapshots of assemblies of CNTs having lengths (I) 15 nm, (II) 28 nm and (III) 43 nm. The bottom panel sketches typical representation of CNT bundles connected by a dendritic network as hypothesized in several literature studies. (B) Conductivity calculated from several hPF-MD simulations of CNTs assembled in templated matrices of lamellar phases of block copolymers; in the right panel two types of CNT assemblies intra-lamellar (pizza shaped) and interfacial (2D dendritic) are highlighted. (C) Joule heating simulation of a CNT assembly, temperature isosurfaces are depicted. Panels (A),(B) reproduced from: Nanoscale, 2016, 8, 15538. https://doi.org/10.1039/C6NR03304K. Panel (C) from: Nanoscale Advances 2020, 2 (8), pp 3164-3180. https://doi.org/10.1039/D0NA00238K.

interactions between them are determined using dynamically generated density fields. In this way, similar to conventional particle-based models, variable concentrations can be represented by simply changing the ratio between water and surfactant molecules.

It is important to note that comparable outcomes were also achieved for different systems; specifically, mixtures of several triblock-copolymers with water at various concentrations have been studied.[82] For the triblock copolymers named Pluronic L62 and L64, in particular, the ability of the hPF models in the accurate reproduction of micellar and non-micellar phases has been investigated. The diverse morphologies that are experimentally observed can be accurately described by hPF models at various polymer concentrations. Moreover, it has been possible to replicate the hexagonal phase of Pluronic L64 but not for L62. While the two copolymers are remarkably similar, in good agreement with several experimental findings, only in the case of L64 a stable hexagonal phase in tiny region of the phase diagram is observed in hPF-MD simulations.

Triton X-100 (TX-100), a common detergent used in biological applications, has been modeled by hPF approach.[83] The critical micelle concentration, shape transition in isotropic micellar phase,[84] and emergence of hexagonal ordered phase in the experimental ranges described in the literature are all reproduced by the coarse-grained (CG) hPF model, which has been accurately validated in a wide range of concentrations. By using a proper reverse mapping procedure, the CG model's fine resolution made it possible to obtain atomistic configurations of micellar assemblies and of the hexagonal phase. Using the same CG model, the complex process of membrane solubilization has been explored in order to validate the mechanism that has been described in the literature. As a series of complex events, it has been possible to simulate a solubilization process that is consistent with the most widely accepted three-stage model (Fig. 5C).[85] Furthermore, based on the rapid or slow detergent partitions, different solubilization paths have been

observed in hPF-MD simulations. The simulated solubilization mechanisms are consistent with experimental data presented by Stuart,[86] Kragh-Hansen,[85] and Lichtenberg's original three-stage model mechanism generalization.[86,87]

CG hPF models close to an atomistic resolution have also been used to study how biomembranes interact with nanoscopic particles like micelles or carbon nanotube (CNT) bundles.[88] Using simulations on the microsecond scale, the formation and insertion/rearrangement of CNTs bundles inside lipid bilayers, which serve as models of biological membranes, have been described and investigated in depth. As depicted in **Fig. 5**(D), lipid molecules coat the surfaces of the bundles during the insertion process, and systems undergoing the insertion of bundles consisting of longer CNTs reveal more significant bilayer distortions. Moreover hPF-MD simulations show lipid adsorption on CNT surfaces causing a transitory poration. This finding suggested a membrane disruption mechanism in which bundles are responsible for creating solvent-rich compartments inside biomembranes.

The most successful block-copolymer micelles in nanomedicines, including those being studied in phase I/II as anticancer agents, are those based on pluronics.[89] hPF-MD simulations of large-scale systems were carried out to investigate the interactions of Pluronic micelles with DPPC lipid bilayers on the microsecond timescale.[90] The migration of Pluronic chains from the micelle to the bilayer has observed in hPF-MD simulations in agreement with the findings from different experimental investigations (**Fig. 5**E). hPF-MD simulations revealed also that the micelle's size is altered by this chains release. According to the simulations, interactions between the drug and the micelle core as well as between the block copolymer and the bilayer contribute to the stability of the micelles. The hydrophobicity of the drug molecules encapsulated in the micelle's core shows a considerable dependence on the equilibrium size of the drug vector.

Fig. 6(A) reports typical conformations of a polyelectrolyte chain in solution at relative dielectric constants. Using hPF-MD extension to charged models the polyelectrolyte chain's globule coil-stretch transition as the dielectric constant grows has been observed in a test model.[54] As shown in **Fig. 6**(B), the chain size at different values of dielectric constant produced by the hPF simulations converges to values obtained by reference MD simulations when the grid size approaches the particle diameter. In addition to the test system previously described, realistic CG models of charged surfactants have been implemented in the same publication.[54] Specifically, the phase separation of PMMA-*b*-PEO block copolymers caused by salt utilizing hPF models with a MARTINI-like mapping scheme has been modeled (**Fig. 6**B). Following the same approach, CG models based on MARTINI-like mapping schemes of sodium dodecyl sulfate (SDS) surfactant and palmitoyloleoylphosphatidylglycerol (POPG) lipid bilayers in an aqueous environment were proposed and validated.[91] These models were then used in comparison to experiments to explain the emergence of micellar morphologies of SDS water solutions at different concentrations.[92] More recently, more elaborate models of the lipids composing the gram-negative bacteria's outer membranes have been developed and validated in the framework of hPF-MD.[93] CG models of biological variants of Lipid A have
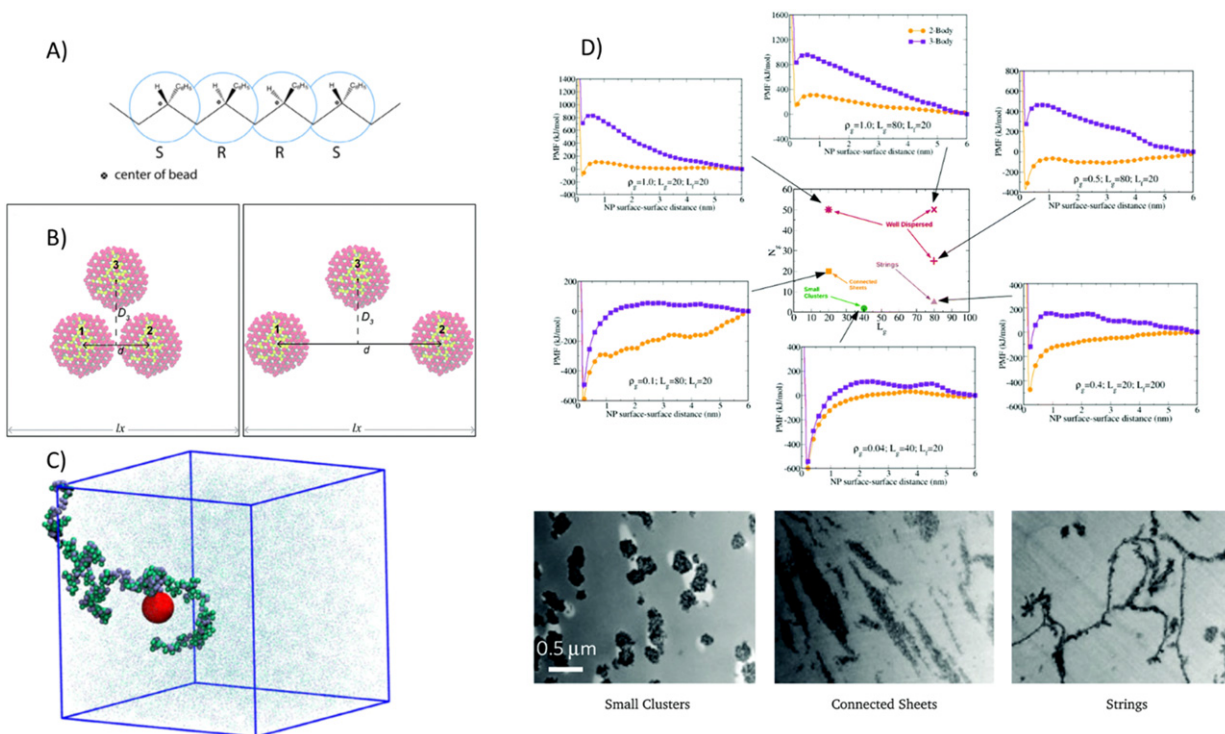
Fig. 8   (A) Mapping scheme for CG model of atactic PS; (B) CG models of Silica NPs distance of separation *d* used for PMF calculations. A third NP is added at a distance D3 to estimate three body effects in the PMF. (C) Typical snapshot of the simulated Silica PS composite, only one chain is shown the remaining chains are depicted using light representation for clarity. (D) Two body and three body PMF for NPs separations calculated using Thermodynamic Integration of hPF-MD simulations. Panels (B), (D) reproduced from: Nanoscale 2018, 10, 21656-21670. https://doi.org/10.1039/C8NR05135F Panels (A), (C) from: Eur. Phys. J. Spec. Top. 2016 225, 1817. https://doi.org/10.1140/epjst/e2016-60127-0.

Fig. 9 (A) Scheme explaining the hierarchical structural organization of CB fillers; (B) Typical chain conformation of polymer chains at a solid surface. Yellow beads belong to train, blue correspond to loop and red to tail conformations. Comparison between top (primary particle) and lower panels (ideal planar graphitic geometry) shows how different are chain arrangements. (C) Different length-scales involved in modeling CB from atomic level up to agglomerat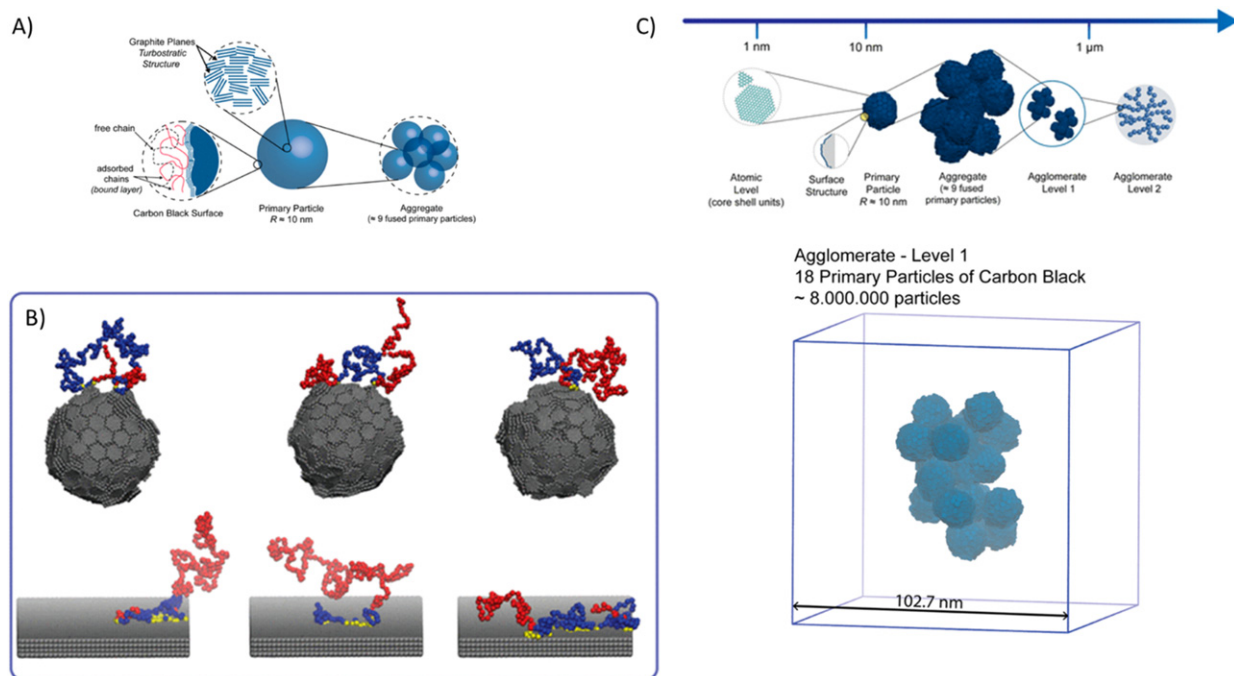e of Level 2. In the bottom panel a model system of an agglomerate of Level 1 embedded in a polymer melt is shown. The optimized version of the massively parallel code OCCAM makes the simulations of systems of this size (about 8 million of beads) routinely. Reproduced from: J. Chem. Theory Comput. 2021, 17, 3, 1755–1770. https://doi.org/10.1021/acs.jctc.0c01095.

been considered (see **Fig. 6**C). More specifically, as shown in **Fig. 6**(D), the stability of Lipid A bilayers for two distinct hexa- and tetra-acylated architectures has been considered. hPF-MD simulations, starting with a randomly dispersed initial distribution of Lipid A molecules with counterions in water, predict the expected self-assembled structures of different lamellar and micellar phases. Moreover, a spontaneous vesiculation process, obtained by fusion micellar aggregates, has been observed.

5.2 Polymer Nanocomposites

To explain the macroscopic characteristics of polymer nanocomposites, such as the dispersion of fillers, heat conductivities, and electrical conductivities, one must have a thorough understanding of the structure of the material on both the chemical and mesoscopic scales. Indeed, both the bulk material and the interfaces affect these characteristics. For instance, the miscibility and level of dispersion in polymers are closely connected to the size of the fillers as well as their surface characteristics. This seems reasonable given that fillers and polymer structure can interact at many levels along the length scales of a typical polymer chain, which range from a single repeating unit (1 nm) to the persistence length to the radius of gyration of an entire chain (30–100 nm). In light of this, it is obvious why models that can account for characteristics from a molecular scale up to a realistic filler size (at least 100 nm) would be highly desirable for this class of materials.

Since CNTs were discovered by Iijima[94] in 1991 and the first polymer nanocomposite with CNTs as a filler were described in 1994,[95] CNTs have attracted a lot of interest in the field of polymer nanocomposites. The dramatic increase in electrical conductivity of nanocomposites around the percolation threshold has recently sparked an increasing interest in percolation of CNT/polymer nano-composites in experimental and theoretical research fields.[96,97] There have been a number of research addressing the percolation process that are based on statistical models of polymer nanocomposites. Monte Carlo (MC) simulations have been used extensively in these investigations[98,99] focused on statistical percolation models, in which fillers are dispersed randomly (i.e., uniformly) throughout the matrix and form percolating clusters as their concentrations is increased. The most important aspects of the percolation process have been studied statistically, however the interactions between the fillers in the matrix are frequently left out and handled using excluded volume conditions (i.e., hard or soft core non-superposition). For CNTs with various aspect ratios, the use of an explicit polymer matrix and the characterization of the simulated structures have been described for the first time using hPF models.[100] To accurately characterize the physics of the CNT assembly and produce the final morphology, the degrees of freedom of the polymer chains must be explicitly included. Indeed, it is expected that entropic effects brought on by the conformational degrees of freedom of the polymer chains would be crucial. In fact, in polymer composites, the chains restricted in the space between the two nanoparticles with high aspect ratios really dominate the free energy of interaction between CNTs. The hPF-MD made possible to simulate large-scale systems
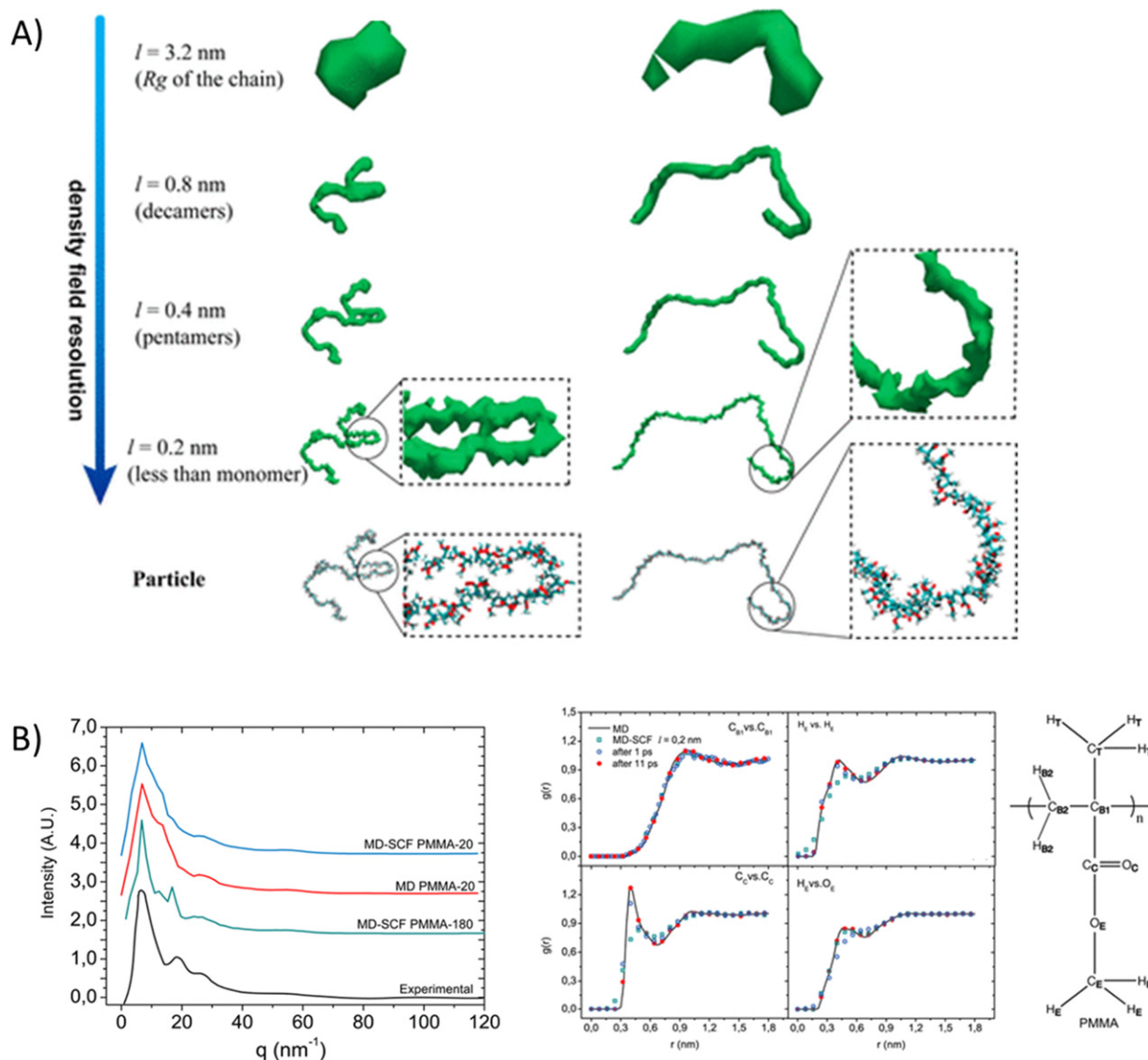
Fig. 10   (A) Isosurfaces calculated from density fields calculated from a chain of PMMA (in two different conformations with grid resolution going from $l = 3.2$ nm $\sim$ Radius of gyration of the chain to $l = 0.2$ nm $<$ submonomer scale). (B) X-ray scattering intensities calculated using hPF-MD procedure compared with very long MD simulations and experiments (left panel); radial distribution functions for several atom pairs together with a scheme showing the repeating unit structure and atom labels. Reproduced from: J. Chem. Theory Comput., 2014, 10 (12), 5651–5667. https://doi.org/10.1021/ct500492h.

(up to 1.5 million beads) with flexible rod-like particles (modeling CNTs) in various matrices consisting of bead spring chains on a millisecond time scale. The equilibrium morphologies for longer CNTs were in good agreement with the results obtained in a number of experiments that postulated a two level "multiscale" structure of CNT assemblies. Morphologies of CNTs assemblies are reported in **Fig. 7**(A). These morphologies have been obtained by hPF-MD starting from homogenous mixtures of CNT and polymer chains. Going from panel (I) (low aspect ratio) to panel (III) (higher aspect ratio) of **Fig. 7**(A) the emergence of dendritic morphologies having CNT bundles connected by few CNTs is apparent. As for electrical properties of the obtained CNTs morphologies, the power laws fitted from experimental results are comparable with the electrical characteristics of the structures determined by hPF models. In particular, for the power law dependence of the electrical conductivity on the CNT fraction, systems close to "kinetic percolation" show exponents close to 1.7, while systems in which the CNTs are homogenously dispersed show exponents close to 2.0, according to the interpretation established by the systematic studies of Bauhofer and Kovacs.[96] In **Fig. 7**(B) the morphologies of templated self-assembled structures of CNT obtained starting from lamellar morphologies of symmetric and incompatible block copolymers are reported.

Using similar models, in a recent paper, the impact that CNT morphologies, concentrations, and working conditions have on Joule heating have been examined and other experiments have been carried out as well using the hPF models as a foundation.[101] The results of targeted tests conducted in conjunction with simulations are in both qualitative and quantitative agreement with
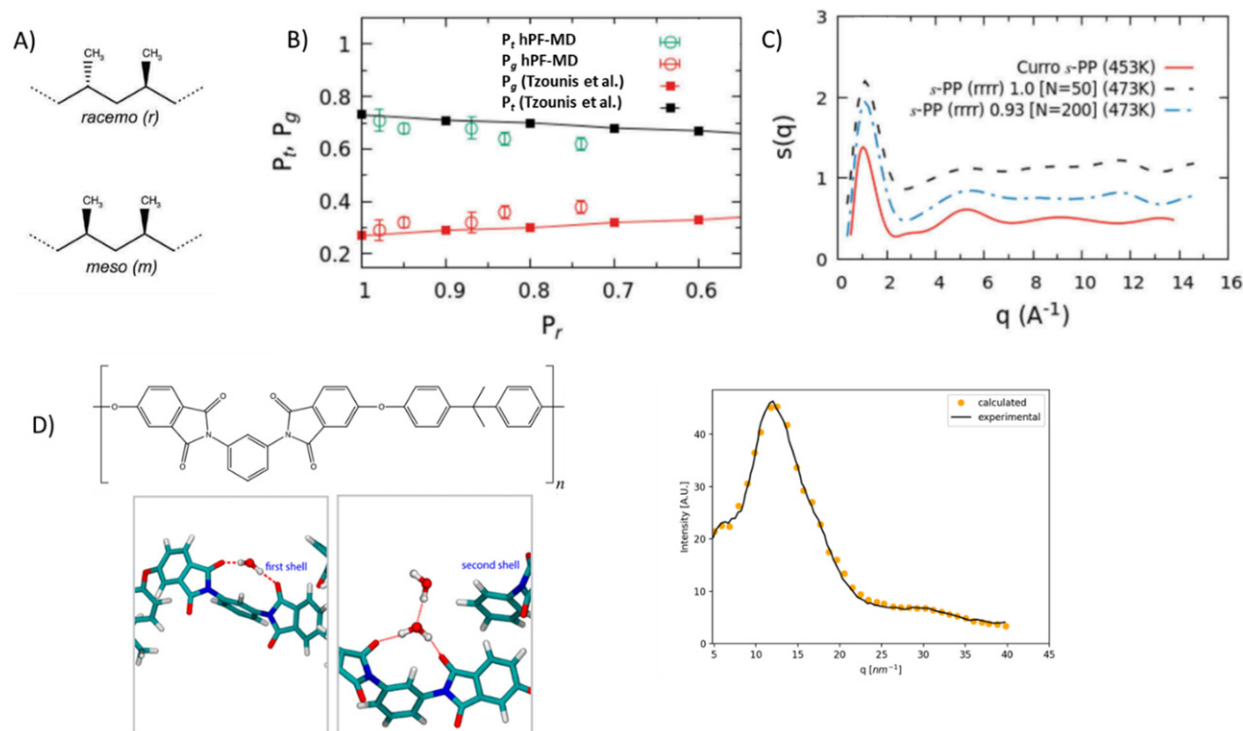
Fig. 11 (A) Racemo r and meso m diads in polypropylene. (B) Fractions of *gauche* and *trans* conformations obtained from hPF-MD simulations compared with literature results of Tzounis *et al.*; (C) Structure factors calculated from hPF-MD simulations for syndiotactic PP compared with experimental data. Plots are shifted to better compare the data. (D) Chemical structure of the repeating unit of PEI; typical arrangements of water molecules at low and high concentrations in PEI (lower panel) and X-ray scattering of PEI all atom model obtained by the procedure of successive hPF-MD equilibrations at different grid resolutions compared with experiments (right panel). Panels (A)-(C) reproduced from: Soft Materials 2020, 18, 228. https://doi.org/10.1080/1539445X.2020.1716801. Panel (D) from: J. Phys. Chem. B 2017, 121 (14), pp 3162–3176. https://doi.org/10.1021/acs.jpcb.7b00992.

studies and trends documented in recent literature. In **Fig. 7**(C) the isosurfaces of temperatures obtained in different regions of CNT assemblies during a simulation of Joule heating after the application of an external electric potential difference are shown.

Due to the large amount of experimental literature, polymer nanocomposites made of silica nanoparticles (NPs) dispersed in atactic polystyrene have been considered as well characterized system[102] to be investigated as test systems for hPF-MD. The mapping scheme adopted for these models (parametrized for intramolecular interactions using IBI to reproduce reference atomistic simulations and for non-bonded interactions to reproduce reference atomistic density profiles) is shown in **Fig. 8**(A), while in **Fig. 8**(B) typical configurations of these systems are shown. In order to examine the interfacial characteristics and potential of mean force (PMF) for separating nanoparticles in a melt, a systematic application of thermodynamic integration (TI) using hPF models of silica NPs has been applied in Ref. 78. Aiming to shed light on the interactions between free and grafted chains (several experimental papers consider silica NPs grafted with the same polymer of the dispersing matrix to increase the compatibility)[103] regulating the dispersion of NPs in the nanocomposite, silica nanoparticles that are either bare or grafted with polystyrene chains have been specifically studied in this work. The wet-brush-to-dry-brush transition is captured by the suggested hybrid models. Moreover these models have shown good abilities to capture the local structure of the chains and, in particular, their density profiles. These models have been used to compute the free energy of separation between pairs of grafted and ungrafted NPs in a polystyrene matrix. In addition, the PMF's three-particle contribution and its role in controlling nanometer-scale phase separation observed in experiments, has been also calculated by including a third particle at a fixed distance in TI calculations. The schematic morphological diagram for grafted NPs embedded in a PS matrix is shown in the figure after computing the second virial coefficient and taking into account the three-body PMF. The corresponding self-assembled structures obtained by transmission electron microscopy are displayed in the same figure. The various experimental morphologies seen at low grafting densities can be well explained by a balance between the two particle and the multi-particle contribution to the PMF. For example, as shown in **Fig. 8**(D), the two body PMF, corresponding to the grafting density where NPs strings are observed, is very attractive at short distances and it keeps to be attractive in the whole range, while the effect of the presence of a third particle makes the PMF positive and repulsive in the whole range. This can explain why arranging NPs in strings can minimize the two particle contribution to free energy without including the three particle repulsive contribution. Later on it has also been investigated how the local structure and with the PMF between silica nanoparticles (NPs) in a polystyrene melt are affected by the bidispersity of polymer chains.[83] The computed trends are quite general and correlate with a number of studies that have been documented in the literature; they are not just applicable to the particular situation of silica-PS nanocomposites. Bidispersity, grafting density, and multibody contact interact in a complicated way, leading to a rich phase behavior that qualitatively matches the experimental data on these systems that are currently available.[104] These

results show that hPF-MD can provide a useful chemically specific computational tool for the research of the composite stability under a wide range of situations since it can capture microscopic interactions at the molecular level.

The most recent use of hPF-MD to simulate polymer composites are CG models made up of carbon black (CB) and polyethylene that are adequate for filler/polymer interactions (PE).[105] In **Fig. 9**(A) a schematization of the hierarchical structure of CB aggregates is depicted. Starting at the lowest scale (atomic or molecular, 1 nm or less), according to the findings of adsorption tests,[106] the surface of CB is distinguished by several adsorption sites. Microcrystallites are arranged spherically in primary particles, with a radius of 10 nm.[107–109] CB fillers are not found in polymer composites as single graphitic units or even as single primary particle. Conversely, the smallest dispersible units in polymeric materials typically consist of two or four primary particles, which are often grouped in clusters of nine to ten (on average) and have a radius of about thirty nanometers (nm). With this in mind, it is clear how, in addition to the surface characteristics of CB (such as the presence of high energy surface sites), the size of the primary particles, the aggregate morphology of a specific CB grade, and the compounding conditions all have a significant impact on the miscibility and degree of dispersion in polymers. In this framework, the computational efficiency of the hPF CG model enabled large-scale simulations of realistically sized (20 nm) CB primary particles embedded in PE melts but, at the same time, describing the details of the CB surface structure. By analyzing the conformational behavior of PE chains adsorbed on various surface regions of CB primary particles, which differs from simplified models based on flat infinite surfaces, it is possible to obtain a detailed description of the bound layers. In **Fig. 9**(B) the conformations of PE chains in contact with the surface of the CB particles are compared with those obtained using idealized flat surfaces. In the same study an optimized version of the OCCAM software for massive MD parallel runs (up to more than 8 million of beads) has also been proposed according to the features of these systems. The computational effectiveness of the optimized code opens up the possibility for a computational screening of the bound layer that takes into account the desirable surface chemistry, size, and shape of CB aggregates, and the molecular weight distribution of the polymers, resulting in a significant tool to address the polymer/fillers interface and interphase engineering in the polymer industry.

5.3   hPF-MD All-Atom Simulations

Starting from the early studies aimed at accomplishing molecular/atomistic scale relaxed structures of dense polymer melts, two main challenges are still subject of intense research and must be addressed: (1) Appropriate coarse-graining methods, which entails developing a mapping scheme and related automated protocols to incorporate features from all-atom reference simulations; (2) the appropriate back-mapping strategy to arrive at reliable all-atom configurations. For a very recent and comprehensive review of polymer multiscale simulation, the reader can refer to Ref. 35.

Initial applications of all-atom hPF-MD simulations have been made to achieve this goal. A strategy that produces well-relaxed all-atom structures of polymer melts has been applied to melts of poly(methyl methacrylate) (PMMA) and poly(ethylene oxide) (PEO) as test systems,[110] and later to polypropylene at various tacticities.[111] In **Fig. 10**(A) the equilibration procedure, consisting in successive MD simulations using different density grid resolutions, is schematized for PMMA. Using this approach all-atom structures with structural correlations identical to those obtained by lengthy MD relaxations have been obtained, demonstrating that even subtle effects on the final melt structures can be adequately described. The suggested method results in computational costs that are more closely related to system size than to chain length, indeed due to the softness of hPF forces, chains can cross each other. Beside this, the suggested method has a number of benefits over conventional coarse-graining/reverse mapping techniques. No parametrization is needed to generate relaxed structures of different polymers at different scales or resolutions. To show this, for example in **Fig. 10**(B), radial distribution functions calculated with respect to different atom pairs compared with the ones obtained by long equilibrations using traditional MD are reported. X-ray scattering of all-atom relaxed models obtained from very long MD simulations, experiments and hPF-MD simulations are reported in the same figure. These results show how sensible the hPF approach is towards details of chemical structures if the proper grid resolution is chosen. To better test this issue the same procedure proposed for PMMA and PEO has been applied to polypropylene (PP) in order to understand if fine details of chain topology related stereoregularity (a scheme explaining the meso and racemo diad of PP is reported in **Fig. 11**(A)) and their consequences on the melt structure could be grasped by hPF models. This represents a very hard test for the methodology because structural effects of tacticity are very relevant in the solid crystalline state of polymers, but very tiny for melts, especially if the lateral group of the main chain is small as in PP. In **Fig. 11**(B) the average *trans* and *gauche* conformations fractions are reported as function of the r diad percentage for hPF-MD simulations and compared with literature results of long MD all atom simulations. In **Fig. 11**(C) the experimental structure factors are compared with the ones obtained from hPF-MD simulations. Recently this approach has been also successfully applied to polymers with complicated architectures, containing several rings in the main chain, such as poly-etherimides (PEI). The chemical structure of the repeating units is reported in **Fig. 11**(D) and in the same Figure the calculated X-Ray scattering compared with experiments is also reported. Relaxed all-atom structures utilized to study the behavior of water[112] and carbon dioxide[113] at low activity in comparison with spectroscopic, gravimetric experiments and theoretical models have been obtained for this class of polymers. In **Fig. 11**(D) the typical arrangements of water molecules present in PEI and verified by FTIR measurements are reported.[112] We would like to stress that, differently from traditional CG approaches based on particle reductions, here is no need for special algorithms or back-mapping schemes to change the resolution of the models. Indeed the procedure involves only a change of resolution of the coarse-grained density and all the atoms degrees of freedom are always present during the successive equilibrations. Then there is no need to reinsert them. This characteristic makes the procedure general and its extension to other polymer architectures is straightforward. The generation of all-atom structures of block copolymer melts and polymer nanocomposites could well be accomplished using similar techniques. The reported all-atom results obtained using hPF models look promising and an extensive use of all-atom hPF-MD simulations can be foreseen for the investigation of biomolecules.
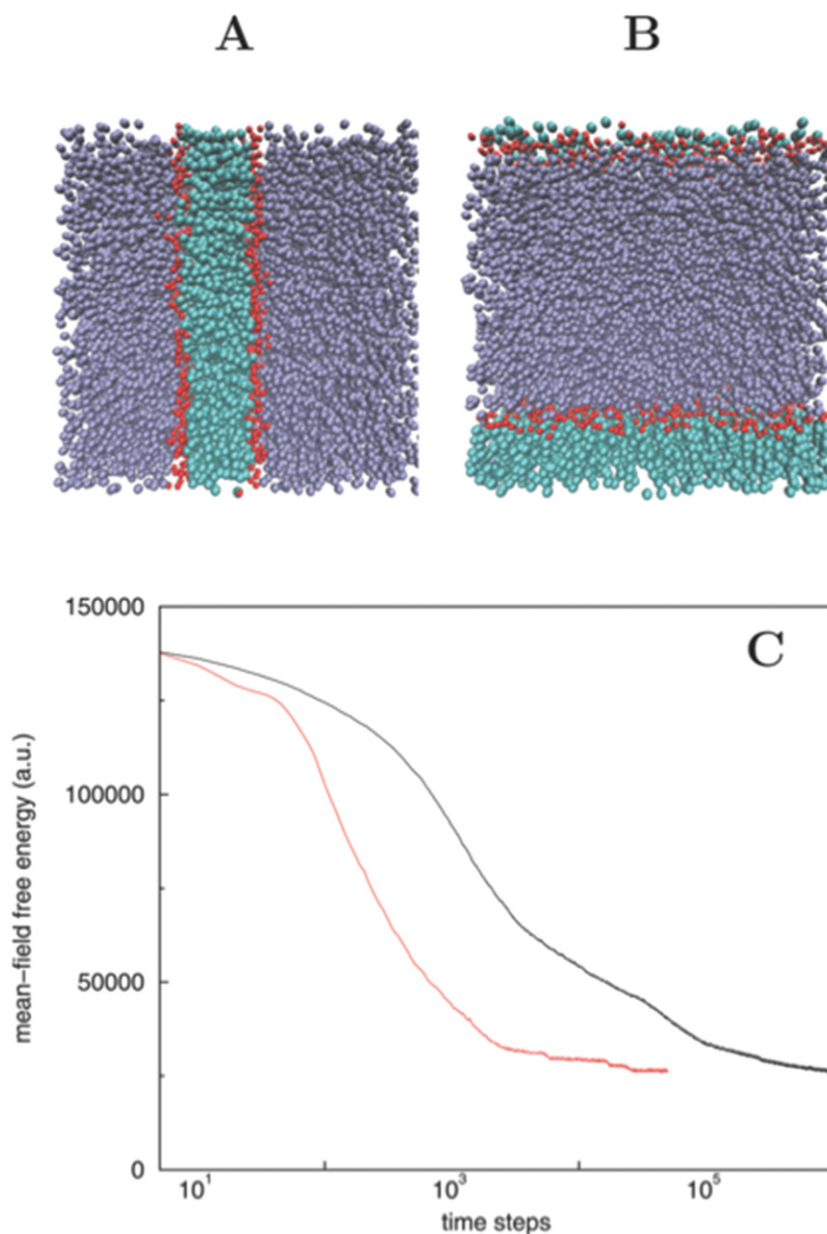
Fig. 12 Snapshots after 50,000 time steps of hPF-MD with MPCD (A) and after 1,000,000 time steps with an Andersen thermostat (B), starting from the same random mixture of lipids (represented as $H_3(C_4)_2$) and water (W). In both cases, flat membranes spanning the $22 \times 22 \times 22$ simulation volume (all in units of r_c, $n_l = 764$, $\Delta t^* = 0.01$) are formed. All particles are shown, with red/blue/iceblue representing H/C/W particles. (C) Comparison of the evolution (logarithmic time axis) of the mean-field free energy $W[\phi]$ for the self-assembled membranes shown above (red: MPCD, black: Andersen thermostat). Reproduced from: Soft Matter, 2017, 13, 1594-1623. https://doi.org/10.1039/C6SM02252A.

6   Dynamics

Analysing the evolution of a system from simulated CG trajectories can be challenging; more generally, the kinetic description in CG methodologies should be considered with some care. hPF-MD is no exception. The effective acceleration of particles (effective beads or atoms) motion compared to the corresponding atomistic models is caused by several factors. Among others, the softening of interactions that comes with coarsening lowers the energetic barriers for important stochastic events, for instance the escape from a molecular cage, which illustrates that smoother energy landscapes result in a reduced effective bead friction owing to smoother forces involved in non-bonded interactions. Moreover, according to the equipartition theorem, thermal energy is distributed over a different number of degrees of freedom. A practical way to match time scales of hPF-MD simulations, provided that the scaling is linear, is by direct comparison of dynamical properties determined using hPF and atomistic simulations. One approach, previously applied to models derived by IBI, is to
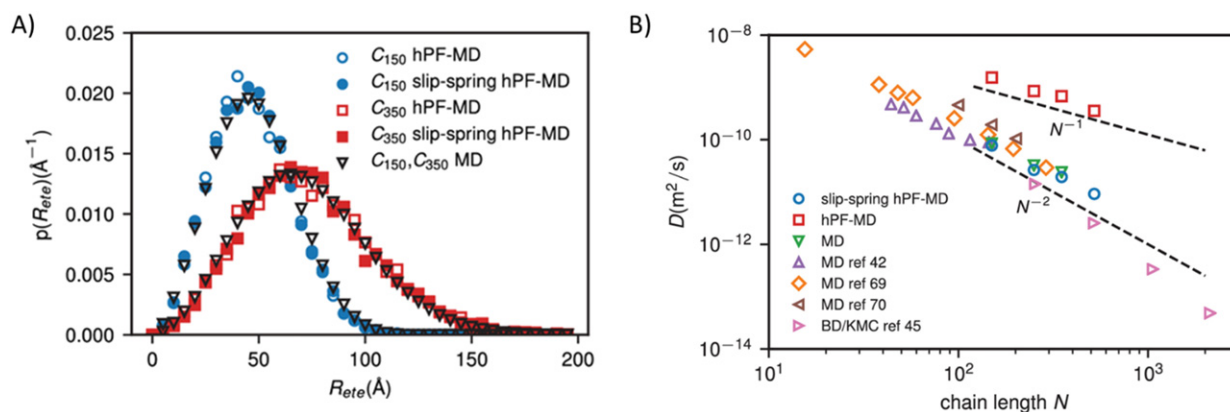
Fig. 13   (A) Distribution of end-to-end distance for atomistic models of polyethylene. Results from hPF-MD (hollow), slip-spring hPF-MD (filled), and MD (black) simulations are compared. (B) Scaling behavior of the diffusion coefficients as function of number of repeating units. For hPF-MD simulations (red squares), diffusion coefficients scale as $\sim N^{-1}$; For slip-spring hPF-MD simulations (blue circles), the diffusion coefficients scales as N^{-2}; The results are compared with traditional MD simulations (green inverted triangle) and other MD simulations of polyethylene melts made using pair potentials. Reproduced from: J Comput Chem. 2021. 42, 6–18. https://doi.org/10.1002/jcc.26428.

compare the diffusion coefficients estimated from atomistic simulations with coarse-grained models, which, for several models of surfactants, provided a speedup factor of about 20.[114] This type of straightforward scaling can be useful to have a semi-quantitative idea of the relevant timescales, but a lot of care has to be taken if dynamical properties need to be obtained from hPF models. Indeed, the complexity in soft matter systems is the multitude of energy barriers that are all approximately equal in height, and a common issue is that typically all barriers are not decreased in the same manner by the CG representation. A correct description of dynamics is rooted in the consideration of the important physical ingredients related to the systems under consideration. Here we give two examples, one related to the incorporation of long-range hydrodynamic interactions and a second related to the dynamics of polymer melts in entangled regime.

One of the most attractive aspects of computationally-efficient hybrid methodology is that simulations may be started quite far from the actual structure or situation that one is really interested in, in some relevant metric, owing to the fact that the sampling of phase space is significantly enhanced (or more ergodic) compared to standard particle-based methods. Especially in soft matter systems, where the thermodynamic driving forces for structural transitions are rather small, this is a very advantageous attribute, as it offers a straightforward solution for dealing with biases that may be introduced by the choice of the initial setup. From the viewpoint of a realistic kinetic description, re-introducing factors that are affected by the smoothing employed in hPF-MD, for instance, the effects of particular particle correlations that are at the basis of entanglement and the discussed caging phenomenon in standard particle-based methods, is an important goal. In addition, including the long-range (hydrodynamic) interactions that are known to considerably speed up the phase separation dynamics is both important for a more realistic dynamic representation and for maximizing the sampling rate in phase space.

The standard course of action in setting up a computational evaluation of any soft matter system is to first perform simulation in a *NPT* ensemble, generally using a barostat that brings the system to a desired pressure, followed by *NVT* ensemble simulation. Options for hybrid simulation at constant pressure have been discussed in an earlier section. Next, we discuss the thermostat that is needed for performing hPF-MD simulations in an *NVT* ensemble. For additional background material and references to related literature we refer to a published study.[115]

A key requirement for the choice of the thermostat in hPF-MD is that the *decoupling* between particles located on different molecules is conserved, since it enables calculation of non-bonded interactions between many particles via a few global fields. It is exactly this attribute that most contributes to the high efficiency of hPF-MD when compared to standard particle-based approaches at the same resolution, see the section about Implementation. The other factor, the time step, is constrained by intramolecular bond stretching, and thus in most cases it is not affected by the smoothing due to the hybridization. Unfortunately, most available thermostats that are Galilean invariant, i.e., momentum conserving and thus accounting for hydrodynamics,[116] including the Lowe–Andersen[117] and the Nosé–Hoover thermostat,[118,119] are based on velocity-differences between pairs of particles. By requiring a so-called neighbor list, which dynamically keeps track of all particle neighbors within a certain Euclidian distance, they violate this important requirement for efficient implementation.

The so-called local Andersen thermostat,[120] which resets the velocity of a set of randomly selected particles in order to maintain a preferred temperature via the Maxwell-Boltzmann distribution, is one of the options that does not require particle pairs, and thus most applications of hPF-MD up to this moment have employed this thermostat. Unfortunately, the second desired property, momentum conservation, is not satisfied by this simple thermostat. The most apparent consequence of this violation of Galilean invariance can be seen in hPF-MD simulations of aggregation. In the absence of other longer-ranged interactions, e.g. electrostatics, the rate with which structure coarsens is rather sensitive to hydrodynamics, and motion (and thus coalescence of small aggregates) slows down considerably with increasing aggregate size.

A decoupled solution to the issue of momentum conservation, and a way to re-introduce the particle 'entanglement' that is automatically present in particle-based methods, is Multi-Particle Collision Dynamics (MPCD).[121] This discrete-time method was originally defined for point-like particles that only kinetically interact by undergoing streaming (ballistic motion) and collision (momentum exchange) steps, in the absence of the usual interaction potentials. Collisions take place in a grid of computational cells, and since only the center of mass velocity of each cell needs to be calculated for the collision, that is also thermostated, pair interactions are not needed.[121] In particular, the streaming step is given by

$$r_i(t + \delta t) = r_i(t) + v_i(t)\delta t \tag{20}$$

for each particle indexed by i, with δt the time increment between collisions, r_i the particle positions and v_i. their velocities. Given the center of mass velocity for n_c particles in a cell of size $a \times a \times a$ given by

$$v_{cm} = \frac{1}{n_c} \sum_{j=1}^{n_c} v_j \tag{21}$$

the velocity update for each of the n_c particles is given by

$$v_i = v_{cm} + R(v_i - v_{cm}) \tag{22}$$

with R a 3×3 matrix that rotates vectors by a fixed angle α around an axis that is randomly selected for each cell. It was shown that MPCD is Galilean invariant if cells are additionally shifted by a small random vector prior to collision.[122] The Green-Kubo relations can be used to derive hydrodynamic properties in terms of n_c (or a), α, and δt, establishing a link between these parameters and actual systems. In hPF-MD/MPCD, the streaming step is replaced by the standard position update of MD.[115] The key choice, currently still under consideration, for applying MPCD to an *interacting* solvent/solute system like a lipid membrane is whether the rotation in the collision step should be applied only to the solvent or to the solute as well.

Application of hFP-MD/MPCD to a single-particle system ($\chi = 0$) in which particles only experience excluded volume interactions characterized by a chosen κ value, showed that introducing collisions by MPCD gives rise to fluctuations in the velocity-autocorrelation function (VACF) and negative values at short time scales, reflecting caging.[115] Moreover, with decreasing κ, or for less compressible systems, this effect is amplified, as expected. Direct comparison of the system evolution between hPF-MD with an Andersen thermostat and using MPCD, see **Fig. 12**, shows that the introduction of long-range hydrodynamic interactions via MPCD indeed substantially speeds up the formation of a membrane.[115]

Due to chain crossability, the entangled dynamics of polymer melts is lost in hPF-MD simulations. Chains can cross because the non-bonded interactions are essentially soft-core due to the field treatment. To mimic the topological limitations of entanglements, a multi-chain slip-spring model[124] into the hPF scheme has been included.[123] The addition of slip-springs had little impact on the polymer chains' structure (see **Fig. 13**A), which is compatible with that of typical MD simulations, this approach has been also proved for the knotting behavior of polymer chains[125] and for branched polymers.[126] During long timeframes, dynamical characteristics including mean-square displacements and reorientational relaxation times are in good agreement with conventional MD simulations and theoretical predictions (see **Fig. 13**B), despite the modest deviations observed at short times. A similar approach can be also applied to hPF simulations of CG models having effective beads representing a specific polymer. In particular, the hPF-MD approach has been combined with a frequency-controlled slip-spring model using a CG model.[127] This useful combination of slip-spring and hPF representation of polymer models has been named as RoBerTo approach. Using this set up, a reptation behavior can be clearly observed consistently with the predictions of the tube theory, and with a quantitative prediction power using a parameterization strategy from existing experimental or simulation data.

7   Conclusions

In the nearly fifteen years since the publication of the first paper on hPF-MD,[50] several extensions, improvements, and sophisticated applications have been made. The hPF-MD formulation, its extension to charged systems, to solid nanoparticles and other technical improvements of this methodology allowed applications to several classes of systems. Models with high chemical detail (such as atomistic models or CG with near atomistic resolution) have been explored on time and length scales that are generally inaccessible to equivalent models based on pair potentials. Test applications have been explored for several systems such as biological lipids, surfactants, synthetic polymers and proteins. One attractive feature of hPF-MD is the ability to import intra-molecular interaction terms from traditional MD simulations (based on representation of all atoms or coarse-grained beads) and to extend their applicability through a mean-field treatment of non-bonded interactions. Many challenges and different aspects of this research field need to be addressed in the future. The development of functionals able to correctly describe the physics of the specific problems under investigation is an important task. Some efforts have been already addressed in this direction, but, due to the various applications and the rapid diffusion of hPF-MD technique, the need of new or modified functionals will increase. The majority of hPF-MD applications have been produced using CG representations, although a few applications (targeted to synthetic polymers), obtained using all-atom models, have yielded encouraging results. This suggests continuing to develop and apply all-atom models. This will encourage the creation of new strategies better suited to the atomic scale in addition to the importation of numerous techniques currently established for atomic scale MD simulations. The development of physically inspired techniques to accurately represent the dynamics as function of the degree of coarse-graining of the hPF models will be a highly intriguing issue

following the here described promising attempts. All these interesting targets can be reached including more researchers now outside the small community that develops, validates, and employs hPF methodologies. For this reason, the lack of reliable and efficient freely accessible simulation engines for many of the recent improvements should be addressed because it makes the application extremely difficult for non-experts. This need is not confined to hPF methodologies but is more general and involves all the community developing coarse-graining approaches in molecular simulations.[128]

8   Further Reading

This section is intended to guide the reader to the basics of hPF-MD. A good introduction to SCF Theory is the book "Statistical Physics of Polymers", reference 37 of the bibliography of this chapter. In particular, the third chapter is a smooth introduction to field theory including also essential mathematical tools needed to follow the derivations. After being used with the book previously mentioned, papers[50] and[66] contain all useful information on the formulation of hPF-MD and its implementation in computer codes. As for the parametrization of mean field models, in paper[67] an approach and the relative formulas able to translate parameters of CG models like MARTINI in corresponding χ parameters is provided. For more specific points the body of the chapter contains the basic information and the relative bibliography.

Relevant Websites

The website of OCCAM contains the main information about input format and code usage. The name OCCAM is not an acronym but it is the latinized spelling Ockham. William of Ockham, also known as the "Doctor Invincibilis", was an English Franciscan friar. He is considered to be one of the major figures of medieval thought. Among many things, he is known for his OCCAM razor: "*Frustra fit per plura quod potest fieri per pauciora*". The Occam's razor can be considered as the first statement of a "Coarse Graining Philosophy".

Researchers interested in becoming users and/or code developers can contact giuseppe.milano@unina.it

OCCAM website

https://sites.google.com/view/occammd

References

1. Alder, B.J., Wainwright, T.E., 1957. Phase transition for a hard sphere system. The Journal of Chemical Physics 27 (5), 1208–1209. https://doi.org/10.1063/1.1743957.
2. Alder, B.J., Wainwright, T.E., 1959. Studies in molecular dynamics. I. General method. The Journal of Chemical Physics 31 (2), 459–466. https://doi.org/10.1063/1.1730376.
3. Rahman, A., 1964. Correlations in the motion of atoms in liquid argon. Physical Review 136 (2A), A405–A411. https://doi.org/10.1103/PhysRev.136.A405.
4. Rahman, A., Stillinger, F.H., 1971. Molecular dynamics study of liquid water. The Journal of Chemical Physics 55 (7), 3336–3359. https://doi.org/10.1063/1.1676585.
5. Jorgensen, W.L., Maxwell, D.S., Tirado-Rives, J., 1996. Development and testing of the OPLS all-atom force field on conformational energetics and properties of organic liquids. Journal of the American Chemical Society 118 (45), 11225–11236. https://doi.org/10.1021/ja9621760.
6. van Gunsteren, W.F., Berendsen, H.J.C., 1990. Computer simulation of molecular dynamics: Methodology, applications, and perspectives in chemistry. Angewandte Chemie International Edition 29 (9), 992–1023. https://doi.org/10.1002/anie.199009921.
7. Tieleman, D.P., Marrink, S.J., Berendsen, H.J.C., 1997. A computer perspective of membranes: Molecular dynamics studies of lipid bilayer systems. Biochimica et Biophysica Acta ((BBA)) – Reviews on Biomembranes 1331 (3), 235–270. https://doi.org/10.1016/S0304-4157(97)00008-7.
8. Battimelli, G., Ciccotti, G., Greco, P., 2020. Computer Meets Theoretical Physics: The New Frontier of Molecular Simulation; The Frontiers Collection. Cham: Springer.
9. van Gunsteren, W.F., Dolenc, J., Mark, A.E., 2008. Molecular simulation as an aid to experimentalists. Current Opinion in Structural Biology 18 (2), 149–153. https://doi.org/10.1016/j.sbi.2007.12.007.
10. Shevlin, S., Castro, B., Li, X., 2021. Computational materials design. Nature Materials 20 (6), https://doi.org/10.1038/s41563-021-01038-8. (727–727).
11. De Nicola, A., Touloupidis, V., Kanellopoulos, V., Albunia, A.R., Milano, G., 2022. A combined experimental and molecular simulation study on stress generation phenomena during the Ziegler-Natta polyethylene catalyst fragmentation process. Nanoscale Advances 4 (23), 5178–5188. https://doi.org/10.1039/d2na00406b.
12. Kmiecik, S., Gront, D., Kolinski, M., et al., 2016. Coarse-grained protein models and their applications. Chemical Reviews 116 (14), 7898–7936. https://doi.org/10.1021/acs.chemrev.6b00163.
13. Soares, T.A., Vanni, S., Milano, G., Cascella, M., 2017. Toward chemically resolved computer simulations of dynamics and remodeling of biological membranes. Journal of Physical Chemistry Letters 8 (15), 3586–3594. https://doi.org/10.1021/acs.jpclett.7b00493.
14. Bigay, J., Antonny, B., 2012. Curvature, lipid packing, and electrostatics of membrane organelles: Defining cellular territories in determining specificity. Developmental Cell 23 (5), 886–895. https://doi.org/10.1016/j.devcel.2012.10.009.
15. Kozlov, M.M., Campelo, F., Liska, N., et al., 2014. Mechanisms shaping cell membranes. Current Opinion in Cell Biology 29, 53–60. https://doi.org/10.1016/j.ceb.2014.03.006.
16. Doi, M., 2003. OCTA (Open computational tool for advanced material technology). Macromolecular Symposia 195 (1), 101–108. https://doi.org/10.1002/masy.200390110.
17. Kremer, K., Müller-Plathe, F., 2002. Multiscale simulation in polymer science. Molecular Simulation 28 (8–9), 729–750. https://doi.org/10.1080/0892702021000002458.
18. Baschnagel, J., Binder, K., Doruker, P., et al., 2000. Bridging the gap between atomistic and coarse-grained models of polymers: Status and perspectives. In viscoelasticity, atomistic models, statistical chemistry. In: Abe, A., Albertsson, A.-C., Cantow, H.-J., et al. (Eds.), Advances in Polymer Science, vol. 152. Berlin Heidelberg: Berlin, Heidelberg: Springer, pp. 41–156. https://doi.org/10.1007/3-540-46778-5_2.
19. Groot, R.D., Warren, P.B., 1997. Dissipative particle dynamics: Bridging the gap between atomistic and mesoscopic simulation. The Journal of Chemical Physics 107 (11), 4423–4435. https://doi.org/10.1063/1.474784.
20. Marrink, S.J., Risselada, H.J., Yefimov, S., Tieleman, D.P., de Vries, A.H., 2007. The MARTINI force field: Coarse grained model for biomolecular simulations. Journal of Physical Chemistry B 111 (27), 7812–7824. https://doi.org/10.1021/jp071097f.
21. Monticelli, L., Kandasamy, S.K., Periole, X., et al., 2008. The MARTINI coarse-grained force field: Extension to proteins. Journal of Chemical Theory and Computation 4 (5), 819–834. https://doi.org/10.1021/ct700324x.

22. Pizzirusso, A., De Nicola, A., Milano, G., 2016. MARTINI coarse-grained model of triton TX-100 in pure DPPC monolayer and bilayer interfaces. Journal of Physical Chemistry B 120 (16), 3821–3832. https://doi.org/10.1021/acs.jpcb.6b00646.
23. Seo, S., Shinoda, W., 2019. SPICA force field for lipid membranes: Domain formation induced by cholesterol. Journal of Chemical Theory and Computation 15 (1), 762–774. https://doi.org/10.1021/acs.jctc.8b00987.
24. Miyazaki, Y., Okazaki, S., Shinoda, W., 2020. PSPICA: A coarse-grained force field for lipid membranes based on a polar water model. Journal of Chemical Theory and Computation 16 (1), 782–793. https://doi.org/10.1021/acs.jctc.9b00946.
25. Müller-Plathe, F., 2002. Coarse-graining in polymer simulation: From the atomistic to the mesoscopic scale and back. ChemPhysChem 3 (9), 754–769. https://doi.org/10.1002/1439-7641(20020916)3:9 < 754::AID-CPHC754 > 3.0.CO;2-U.
26. Karimi-Varzaneh, H.A., van der Vegt, N.F.A., Müller-Plathe, F., Carbone, P., 2012. How good are coarse-grained polymer models? A comparison for atactic polystyrene. ChemPhysChem 13 (15), 3428–3439. https://doi.org/10.1002/cphc.201200111.
27. Baschnagel, J., Binder, K., Paul, W., et al., 1991. On the construction of coarse-grained models for linear flexible polymer chains: Distribution functions for groups of consecutive monomers. The Journal of Chemical Physics 95 (8), 6014–6025. https://doi.org/10.1063/1.461826.
28. Paul, W., Pistoor, N., 1994. A mapping of realistic onto abstract polymer models and an application to two bisphenol polycarbonates. Macromolecules 27 (5), 1249–1255. https://doi.org/10.1021/ma00083a027.
29. Tschöp, W., Kremer, K., Batoulis, J., Bürger, T., Hahn, O., 1998. Simulation of polymer melts. I. Coarse-graining procedure for polycarbonates. Acta Polymerica 49 (2–3), 61–74. https://doi.org/10.1002/(SICI)1521-4044(199802)49:2/3 < 61::AID-APOL61 > 3.0.CO;2-V.
30. Milano, G., Müller-Plathe, F., 2005. Mapping atomistic simulations to mesoscopic models: A systematic coarse-graining procedure for vinyl polymer chains. Journal of Physical Chemistry B 109 (39), 18609–18619. https://doi.org/10.1021/jp0523571.
31. Peter, C., Kremer, K., 2010. Multiscale simulation of soft matter systems. Faraday Discussions 144, 9–24. https://doi.org/10.1039/B919800H.
32. Noid, W.G., 2013. Perspective: Coarse-grained models for biomolecular systems. The Journal of Chemical Physics 139 (9), 090901. https://doi.org/10.1063/1.4818908.
33. Brini, E., Algaer, E.A., Ganguly, P., et al., 2013. Systematic coarse-graining methods for soft matter simulations − A review. Soft Matter 9 (7), 2108–2119. https://doi.org/10.1039/C2SM27201F.
34. Saunders, M.G., Voth, G.A., 2013. Coarse-graining methods for computational biology. Annual Review of Biophysics 42 (1), 73–93. https://doi.org/10.1146/annurev-biophys-083012-130348.
35. Schmid, F., 2023. Understanding and modeling polymers: The challenge of multiple scales. ACS Polymers Au 3 (1), 28–58. https://doi.org/10.1021/acspolymersau.2c00049.
36. Parr, R.G., Weitao, Y., 1995. Density-Functional Theory of Atoms and Molecules. Oxford University Press. https://doi.org/10.1093/oso/9780195092769.001.0001.
37. Kawakatsu, T., 2004. Statistical physics of polymers: An Introduction. In: Advanced Texts in Physics. Berlin; New York: Springer.
38. Fredrickson, G.H., 2006. The equilibrium theory of inhomogeneous polymers. International Series of Monographs on Physics. Oxford; New York: Clarendon Press; Oxford University Press.
39. Fredrickson, G.H., Ganesan, V., Drolet, F., 2002. Field-theoretic computer simulation methods for polymers and complex fluids. Macromolecules 35 (1), 16–39. https://doi.org/10.1021/ma011515t.
40. Kawakatsu, T., Kawasaki, K., 1990. Hybrid models for the dynamics of an immiscible binary mixture with surfactant molecules. Physica A: Statistical Mechanics and its Applications 167 (3), 690–735. https://doi.org/10.1016/0378-4371(90)90287-3.
41. Kawakatsu, T., Kawasaki, K., Furusaka, M., Okabayashi, H., Kanaya, T., 1993. Late stage dynamics of phase separation processes of binary mixtures containing surfactants. The Journal of Chemical Physics 99 (10), 8200–8217. https://doi.org/10.1063/1.466213.
42. Kawakatsu, T., Kawasaki, K., Furusaka, M., Okabayashi, O., Kanaya, T., 1994. Theories and computer simulations of self-assembling surfactant solutions. Journal of Physics: Condensed Matter 6 (32), 6385–6408. https://doi.org/10.1088/0953-8984/6/32/003.
43. Ginzburg, V.V., Qiu, F., Paniconi, M., et al., 1999. Simulation of hard particles in a phase-separating binary mixture. Physical Review Letters 82 (20), 4026–4029. https://doi.org/10.1103/PhysRevLett.82.4026.
44. Ginzburg, V.V., Peng, G., Qiu, F., Jasnow, D., Balazs, A.C., 1999. Kinetic model of phase separation in binary mixtures with hard mobile impurities. Physical Review E 60 (4), 4352–4359. https://doi.org/10.1103/PhysRevE.60.4352.
45. Balazs, A.C., Ginzburg, V.V., Qiu, F., Peng, G., Jasnow, D., 2000. Multi-scale model for binary mixtures containing nanoscopic particles. Journal of Physical Chemistry B 104 (15), 3411–3422. https://doi.org/10.1021/jp993356.
46. Zhu, Y., Ma, Y., 2002. Orientational structures of a phase-separating system under oscillatory particles. The Journal of Chemical Physics 117 (22), 10207–10214. https://doi.org/10.1063/1.1518963.
47. Pinna, M., Pagonabarraga, I., Zvelindovsky, A.V., 2011. Modeling of block copolymer/colloid hybrid composite materials: Modeling of block copolymer/colloid hybrid composite materials. Macromolecular Theory and Simulations 20 (8), 769–779. https://doi.org/10.1002/mats.201100047.
48. Laradji, M., Guo, H., Zuckermann, M.J., 1994. Off-lattice monte carlo simulation of polymer brushes in good solvents. Physical Review E 49 (4), 3199–3206. https://doi.org/10.1103/PhysRevE.49.3199.
49. Daoulas, K.Ch, Müller, M., 2006. Single chain in mean field simulations: Quasi-instantaneous field approximation and quantitative comparison with Monte Carlo simulations. The Journal of Chemical Physics 125 (18), 184904. https://doi.org/10.1063/1.2364506.
50. Milano, G., Kawakatsu, T., 2009. Hybrid particle-field molecular dynamics simulations for dense polymer systems. Journal of Chemical Physics 130 (21), https://doi.org/10.1063/1.3142103.
51. Helfand, E., 1975. Theory of inhomogeneous polymers: Fundamentals of the Gaussian random-walk model. The Journal of Chemical Physics 62 (3), 999–1005. https://doi.org/10.1063/1.430517.
52. Rubinstein, M., Colby, R.H., 2003. Polymer Physics. Oxford; New York: Oxford University Press.
53. Bore, S.L., Milano, G., Cascella, M., 2018. Hybrid particle-field model for conformational dynamics of peptide chains. Journal of Chemical Theory and Computation 14 (2), 1120–1130. https://doi.org/10.1021/acs.jctc.7b01160.
54. Zhu, Y.-L., Lu, Z.-Y., Milano, G., Shi, A.-C., Sun, Z.-Y., 2016. Hybrid particle-field molecular dynamics simulation for polyelectrolyte systems. Physical Chemistry Chemical Physics 18 (14), 9799–9808. https://doi.org/10.1039/c5cp06856h.
55. Milano, G., Kawakatsu, T., 2010. Pressure calculation in hybrid particle-field simulations. Journal of Chemical Physics 133 (21), https://doi.org/10.1063/1.3506776.
56. Zhang, G., Daoulas, K.C., Kremer, K., 2013. A new coarse grained particle-to-mesh scheme for modeling soft matter. Macromolecular Chemistry and Physics 214 (2), 214–224. https://doi.org/10.1002/macp.201200520.
57. Zong, J., Meng, D., 2020. Field-accelerated Monte Carlo simulations in the canonical and isothermal–isobaric ensembles. Journal of Chemical Physics 153 (14), 144104. https://doi.org/10.1063/5.0013627.
58. Bore, S.L., Kolli, H.B., De Nicola, A., et al., 2020. Hybrid particle-field molecular dynamics under constant pressure. Journal of Chemical Physics 152 (18), https://doi.org/10.1063/5.0007445.
59. Sevink, G.J.A., Charlaganov, M., Fraaije, J.G.E.M., 2013. Coarse-grained hybrid simulation of liposomes. Soft Matter 9 (10), 2816. https://doi.org/10.1039/c2sm27492b.
60. Sevink, G.J.A., Blokhuis, E.M., Li, X., Milano, G., 2020. Efficient and realistic simulation of phase coexistence. Journal of Chemical Physics 153 (24), https://doi.org/10.1063/5.0027778.
61. Pagonabarraga, I., Frenkel, D., 2001. Dissipative particle dynamics for interacting systems. The Journal of Chemical Physics 115 (11), 5015–5026. https://doi.org/10.1063/1.1396848.
62. Warren, P.B., 2003. Vapor-liquid coexistence in many-body dissipative particle dynamics. Physical Review E 68 (6), 066702. https://doi.org/10.1103/PhysRevE.68.066702.

63. Hömberg, M., Müller, M., 2010. Main phase transition in lipid bilayers: Phase coexistence and line tension in a soft, solvent-free, coarse-grained model. The Journal of Chemical Physics 132 (15), 155104. https://doi.org/10.1063/1.3369005.
64. Maurits, N.M., van Vlimmeren, B.A.C., Fraaije, J.G.E.M., 1997. Mesoscopic phase separation dynamics of compressible copolymer melts. Physical Review E 56 (1), 816–825. https://doi.org/10.1103/PhysRevE.56.816.
65. Carnahan, N.F., Starling, K.E., 1969. Equation of state for nonattracting rigid spheres. The Journal of Chemical Physics 51 (2), 635–636. https://doi.org/10.1063/1.1672048.
66. Zhao, Y., De Nicola, A., Kawakatsu, T., Milano, G., 2012. Hybrid particle-field molecular dynamics simulations: Parallelization and benchmarks. Journal of Computational Chemistry 33 (8), 868–880. https://doi.org/10.1002/jcc.22883.
67. De Nicola, A., Zhao, Y., Kawakatsu, T., Roccatano, D., Milano, G., 2011. Hybrid particle-field coarse-grained models for biological phospholipids. Journal of Chemical Theory and Computation 7 (9), 2947–2962. https://doi.org/10.1021/ct200132n.
68. Zhu, Y.-L., Liu, H., Li, Z.-W., et al., 2013. GALAMOST: GPU-accelerated large-scale molecular simulation toolkit. Journal of Computational Chemistry 34 (25), 2197–2211. https://doi.org/10.1002/jcc.23365.
69. Schneider, L., Müller, M., 2019. Multi-architecture Monte-Carlo (MC) simulation of soft coarse-grained polymeric materials: Soft coarse grained Monte-Carlo acceleration (SOMA). Computer Physics Communications 235, 463–476. https://doi.org/10.1016/j.cpc.2018.08.011.
70. Lyubartsev, A.P., Laaksonen, A., 1995. Calculation of effective interaction potentials from radial distribution functions: A reverse Monte Carlo approach. Physical Review E 52 (4), 3730–3737. https://doi.org/10.1103/PhysRevE.52.3730.
71. Spyriouni, T., Tzoumanekas, C., Theodorou, D., Müller-Plathe, F., Milano, G., 2007. Coarse-grained and reverse-mapped united-atom simulations of long-chain atactic polystyrene melts: Structure, thermodynamic properties, chain conformation, and entanglements. Macromolecules 40 (10), 3876–3885. https://doi.org/10.1021/ma0700983.
72. Tschöp, W., Kremer, K., Hahn, O., Batoulis, J., Bürger, T., 1998. Simulation of polymer melts. II. From coarse-grained models back to atomistic description. Acta Polymerica 49 (2–3), 75–79. https://doi.org/10.1002/(SICI)1521-4044(199802)49:2/3<75::AID-APOL75>3.0.CO;2-5.
73. Santangelo, G., Di Matteo, A., Müller-Plathe, F., Milano, G., 2007. From mesoscale back to atomistic models: A fast reverse-mapping procedure for vinyl polymer chains. Journal of Physical Chemistry B 111 (11), 2765–2773. https://doi.org/10.1021/jp0662121.
74. Chen, X., Carbone, P., Santangelo, G., et al., 2009. Backmapping coarse-grained polymer models under sheared nonequilibrium conditions. Physical Chemistry Chemical Physics 11 (12), 1977–1988. https://doi.org/10.1039/b817895j.
75. Chung, L.W., Sameera, W.M.C., Ramozzi, R., et al., 2015. The ONIOM method and its applications. Chemical Reviews 115 (12), 5678–5796. https://doi.org/10.1021/cr5004419.
76. Szabó, A., Ostlund, N.S., 1982. Modern Quantum Chemistry: Introduction to Advanced Electronic Structure Theory. New York; London: Free Press; Collier Macmillan.
77. de Nicola, A., Zhao, Y., Kawakatsu, T., Roccatano, D., Milano, G., 2012. Validation of a hybrid MD-SCF coarse-grained model for DPPC in non-lamellar phases. Theoretical Chemistry Accounts 131 (3), 1–16. https://doi.org/10.1007/s00214-012-1167-1.
78. Munaò, G., Pizzirusso, A., Kalogirou, A., et al., 2018. Molecular structure and multi-body potential of mean force in silica-polystyrene nanocomposites. Nanoscale 10 (46), 21656–21670. https://doi.org/10.1039/c8nr05135f.
79. Munaò, G., De Nicola, A., Müller-Plathe, F., et al., 2019. Influence of polymer bidispersity on the effective particle-particle interactions in polymer nanocomposites. Macromolecules 52 (22), 8826–8839. https://doi.org/10.1021/acs.macromol.9b01367.
80. Antonietti, M., Förster, S., 2003. Vesicles and liposomes: A self-assembly principle beyond lipids. Advanced Materials 15 (16), 1323–1333. https://doi.org/10.1002/adma.200300010.
81. Koehl, P., 2006. Electrostatics calculations: Latest methodological advances. Current Opinion in Structural Biology 16 (2), 142–151. https://doi.org/10.1016/j.sbi.2006.03.001.
82. De Nicola, A., Kawakatsu, T., Milano, G., 2013. A hybrid particle-field coarse-grained molecular model for pluronics water mixtures. Macromolecular Chemistry and Physics 214 (17), 1940–1950. https://doi.org/10.1002/macp.201300214.
83. De Nicola, A., Kawakatsu, T., Rosano, C., et al., 2015. Self-assembly of triton X-100 in water solutions: A multiscale simulation study linking mesoscale to atomistic models. Journal of Chemical Theory and Computation 11 (10), 4959–4971. https://doi.org/10.1021/acs.jctc.5b00485.
84. Murakami, W., De Nicola, A., Oya, Y., et al., 2021. Theoretical and computational study of the sphere-to-rod transition of triton X-100 micellar nanoscale aggregates in aqueous solution: Implications for membrane protein purification and membrane solubilization. ACS Applied Nano Materials 4 (5), 4552–4561. https://doi.org/10.1021/acsanm.1c00171.
85. Lichtenberg, D., Ahyayauch, H., Goñi, F.M., 2013. The mechanism of detergent solubilization of lipid bilayers. Biophysical Journal 105 (2), 289–299. https://doi.org/10.1016/j.bpj.2013.06.007.
86. Stuart, M.C.A., Boekema, E.J., 2007. Two distinct mechanisms of vesicle-to-micelle and micelle-to-vesicle transition are mediated by the packing parameter of phospholipid–detergent systems. Biochimica et Biophysica Acta ((BBA)) – Biomembranes 1768 (11), 2681–2689. https://doi.org/10.1016/j.bbamem.2007.06.024.
87. Lichtenberg, D., Ahyayauch, H., Alonso, A., Goñi, F.M., 2013. Detergent solubilization of lipid bilayers: A balance of driving forces. Trends in Biochemical Sciences 38 (2), 85–93. https://doi.org/10.1016/j.tibs.2012.11.005.
88. Sarukhanyan, E., De Nicola, A., Roccatano, D., Kawakatsu, T., Milano, G., 2014. Spontaneous insertion of carbon nanotube bundles inside biomembranes: A hybrid particle-field coarse-grained molecular dynamics study. Chemical Physics Letters 595–596, 156–166. https://doi.org/10.1016/j.cplett.2014.01.057.
89. Duncan, R., Gaspar, R., 2011. Nanomedicine(s) under the Microscope. Molecular Pharmaceutics 8 (6), 2101–2141. https://doi.org/10.1021/mp200394t.
90. De Nicola, A., Hezaveh, S., Zhao, Y., et al., 2014. Micellar drug nanocarriers and biomembranes: How do they interact? Physical Chemistry Chemical Physics 16 (11), 5093–5105. https://doi.org/10.1039/c3cp54242d.
91. Kolli, H.B., De Nicola, A., Bore, S.Lø., et al., 2018. Hybrid particle-field molecular dynamics simulations of charged amphiphiles in an aqueous environment. Journal of Chemical Theory and Computation 14 (9), 4928–4937. https://doi.org/10.1021/acs.jctc.8b00466.
92. Schäfer, K., Kolli, H.B., Killingmoe Christensen, M., et al., 2020. Supramolecular packing drives morphological transitions of charged surfactant micelles. Angewandte Chemie - International Edition 59 (42), 18591–18598. https://doi.org/10.1002/anie.202004522.
93. De Nicola, A., Soares, T.A., Santos, D.E.S., et al., 1865. Aggregation of Lipid A variants: A hybrid particle-field model. Biochimica et Biophysica Acta - General Subjects 2021 (4), https://doi.org/10.1016/j.bbagen.2020.129570.
94. Iijima, S., 1991. Helical microtubules of graphitic carbon. Nature 354 (6348), 56–58. https://doi.org/10.1038/354056a0.
95. Ajayan, P.M., Stephan, O., Colliex, C., Trauth, D., 1994. Aligned carbon nanotube arrays formed by cutting a polymer resin—nanotube composite. Science 265 (5176), 1212–1214. https://doi.org/10.1126/science.265.5176.1212.
96. Bauhofer, W., Kovacs, J.Z., 2009. A review and analysis of electrical percolation in carbon nanotube polymer composites. Composites Science and Technology 69 (10), 1486–1498. https://doi.org/10.1016/j.compscitech.2008.06.018.
97. Mutiso, R.M., Winey, K.I., 2015. Electrical properties of polymer nanocomposites containing rod-like nanofillers. Progress in Polymer Science 40, 63–84. https://doi.org/10.1016/j.progpolymsci.2014.06.002.
98. Mutiso, R.M., Sherrott, M.C., Li, J., Winey, K.I., 2012. Simulations and generalized model of the effect of filler size dispersity on electrical percolation in rod networks. Phys. Rev. B 86 (21), 214306. https://doi.org/10.1103/PhysRevB.86.214306.
99. Dalmas, F., Dendievel, R., Chazeau, L., Cavaillé, J.-Y., Gauthier, C., 2006. Carbon nanotube-filled polymer composites. Numerical simulation of electrical conductivity in three-dimensional entangled fibrous networks. Acta Materialia 54 (11), 2923–2931. https://doi.org/10.1016/j.actamat.2006.02.028.
100. Zhao, Y., Byshkin, M., Cong, Y., et al., 2016. Self-assembly of carbon nanotubes in polymer melts: simulation of structural and electrical behaviour by hybrid particle-field molecular dynamics. Nanoscale 8 (34), 15538–15552. https://doi.org/10.1039/c6nr03304k.
101. Donati, G., De Nicola, A., Munaò, G., et al., 2020. Simulation of self-heating process on the nanoscale: A multiscale approach for molecular models of nanocomposite materials. Nanoscale Advances 2 (8), 3164–3180. https://doi.org/10.1039/d0na00238k.
102. Akcora, P., Liu, H., Kumar, S.K., et al., 2009. Anisotropic self-assembly of spherical polymer-grafted nanoparticles. Nature Mater 8 (4), 354–359. https://doi.org/10.1038/nmat2404.

103. Green, D.L., Mewis, J., 2006. Connecting the wetting and rheological behaviors of poly(dimethylsiloxane)-grafted silica spheres in poly(dimethylsiloxane) melts. Langmuir 22 (23), 9546–9553. https://doi.org/10.1021/la061136z.

104. Natarajan, B., Neely, T., Rungta, A., Benicewicz, B.C., Schadler, L.S., 2013. Thermomechanical properties of bimodal brush modified nanoparticle composites. Macromolecules 46 (12), 4909–4918. https://doi.org/10.1021/ma400553c.

105. Caputo, S., Hristov, V., Nicola, A.D., et al., 2021. Efficient hybrid particle-field coarse-grained model of polymer filler interactions: Multiscale hierarchical structure of carbon black particles in contact with polyethylene. Journal of Chemical Theory and Computation 17 (3), 1755–1770. https://doi.org/10.1021/acs.jctc.0c01095.

106. Schröder, A., Klüppel, M., Schuster, R.H., Heidberg, J., 2002. Surface energy distribution of carbon black measured by static gas adsorption. Carbon 40 (2), 207–210. https://doi.org/10.1016/S0008-6223(01)00175-0.

107. Heinrich, G., Vilgis, T.A., 1995. Physical adsorption of polymers on disordered filler surfaces. Rubber Chemistry and Technology 68 (1), 26–36. https://doi.org/10.5254/1.3538729.

108. Donnet, J.-B., Bansal, R.C., Wang, M.-J., 2018. In: Donnet, J.-B. (Ed.), Carbon black: Science and Technology, second ed. Routledge. https://doi.org/10.1201/9781315138763.

109. Takenaka, M., 2013. Analysis of structures of rubber-filler systems with combined scattering methods. Polymer Journal 45 (1), 10–19. https://doi.org/10.1038/pj.2012.187.

110. De Nicola, A., Kawakatsu, T., Milano, G., 2014. Generation of well-relaxed all-atom models of large molecular weight polymer melts: A hybrid particle-continuum approach based on particle-field molecular dynamics simulations. Journal of Chemical Theory and Computation 10 (12), 5651–5667. https://doi.org/10.1021/ct500492h.

111. De Nicola, A., Munaò, G., Grizzuti, N., et al., 2020. Generation of well relaxed all atom models of stereoregular polymers: A validation of hybrid particle-field molecular dynamics for polypropylene melts of different tacticities. Soft Materials 18 (2–3), 228–241. https://doi.org/10.1080/1539445X.2020.1716801.

112. De Nicola, A., Correa, A., Milano, G., et al., 2017. Local structure and dynamics of water absorbed in poly(ether imide): A hydrogen bonding anatomy. Journal of Physical Chemistry B 121 (14), 3162–3176. https://doi.org/10.1021/acs.jpcb.7b00992.

113. Scherillo, G., Mensitieri, G., Baldanza, A., et al., 2022. Weak interactions between poly(ether imide) and carbon dioxide: A multiscale investigation combining experiments, theory, and simulations. Macromolecules 55 (24), 10773–10787. https://doi.org/10.1021/acs.macromol.2c01382.

114. Milano, G., Kawakatsu, T., De Nicola, A., 2013. A hybrid particle-field molecular dynamics approach: A route toward efficient coarse-grained models for biomembranes. Physical Biology 10 (4), https://doi.org/10.1088/1478-3975/10/4/045007.

115. Sevink, G.J.A., Schmid, F., Kawakatsu, T., Milano, G., 2017. Combining cell-based hydrodynamics with hybrid particle-field simulations: Efficient and realistic simulation of structuring dynamics. Soft Matter 13 (8), 1594–1623. https://doi.org/10.1039/c6sm02252a.

116. Stoyanov, S.D., Groot, R.D., 2005. From molecular dynamics to hydrodynamics: A novel Galilean invariant thermostat. The Journal of Chemical Physics 122 (11), 114112. https://doi.org/10.1063/1.1870892.

117. Lowe, C.P., 1999. An alternative approach to dissipative particle dynamics. Europhysics Letters 47 (2), 145–151. https://doi.org/10.1209/epl/i1999-00365-x.

118. Nosé, S., 1984. A unified formulation of the constant temperature molecular dynamics methods. The Journal of Chemical Physics 81 (1), 511–519. https://doi.org/10.1063/1.447334.

119. Hoover, W.G., 1985. Canonical dynamics: Equilibrium phase-space distributions. Physical Review A 31 (3), 1695–1697. https://doi.org/10.1103/PhysRevA.31.1695.

120. Tanaka, H., Nakanishi, K., Watanabe, N., 1983. Constant temperature molecular dynamics calculation on Lennard-Jones fluid and its application to water[a]. The Journal of Chemical Physics 78 (5), 2626–2634. https://doi.org/10.1063/1.445020.

121. Allahyarov, E., Gompper, G., 2002. Mesoscopic solvent simulations: Multiparticle-collision dynamics of three-dimensional flows. Phys. Rev. E 66 (3), 036702. https://doi.org/10.1103/PhysRevE.66.036702.

122. Ihle, T., Kroll, D.M., 2003. Stochastic rotation dynamics. I. Formalism, Galilean invariance, and Green-Kubo relations. Physical Review E 67 (6), 066705. https://doi.org/10.1103/PhysRevE.67.066705.

123. Wu, Z., Kalogirou, A., De Nicola, A., Milano, G., Müller-Plathe, F., 2021. Atomistic hybrid particle-field molecular dynamics combined with slip-springs: Restoring entangled dynamics to simulations of polymer melts. Journal of Computational Chemistry 42 (1), 6–18. https://doi.org/10.1002/jcc.26428.

124. Langeloth, M., Masubuchi, Y., Böhm, M.C., Müller-Plathe, F., 2013. Recovering the reptation dynamics of polymer melts in dissipative particle dynamics simulations via slip-springs. The Journal of Chemical Physics 138 (10), 104907. https://doi.org/10.1063/1.4794156.

125. Wu, Z., Alberti, S.A.N., Schneider, J., Müller-Plathe, F., 2021. Knotting behaviour of polymer chains in the melt state for soft-core models with and without slip-springs. Journal of Physics: Condensed Matter 33 (24), 244001. https://doi.org/10.1088/1361-648X/abef25.

126. Wu, Z., Müller-Plathe, F., 2022. Slip-spring hybrid particle-field molecular dynamics for coarse-graining branched polymer melts: Polystyrene melts as an example. Journal of Chemical Theory and Computation 18 (6), 3814–3828. https://doi.org/10.1021/acs.jctc.2c00107.

127. Wu, Z., Milano, G., Müller-Plathe, F., 2021. Combination of hybrid particle-field molecular dynamics and slip-springs for the efficient simulation of coarse-grained polymer models: Static and dynamic properties of polystyrene melts. Journal of Chemical Theory and Computation 17 (1), 474–487. https://doi.org/10.1021/acs.jctc.0c00954.

128. Sevink, G.J.A., Liwo, J.A., Asinari, P., et al., 2020. Unfolding the Prospects of Computational (Bio)Materials Modeling. Journal of Chemical Physics 153 (10), https://doi.org/10.1063/5.0019773.